Journal for ImmunoTherapy of Cancer

Deconvolution of malignant pleural effusions immune landscape unravels a novel macrophage signature associated with worse clinical outcome in lung adenocarcinoma patients

Sara Bruschini,[1,2] Matteo Pallocca,[3] Eleonora Sperandio,[3] Lorenzo D'Ambrosio,[4] Francesca Ascenzi,[5] Claudia De Vitis,[5] Valentina Salvati,[6] Antonella Esposito,[1] Simona Di Martino,[7] Francesca De Nicola,[8] Francesca Paolini,[4,9] Luigi Fattore,[8] Gabriele Alessandrini,[10] Francesco Facciolo,[10] Maria Laura Foddai,[11] Massimiliano Bassi,[12] Federico Venuta,[12] Michela D'Ascanio,[5] Alberto Ricci,[5] Antonio D' Andrilli,[13] Christian Napoli,[14] Luigi Aurisicchio,[15] Maurizio Fanciulli,[8] Erino Angelo Rendina,[13] Gennaro Ciliberto ,[16] Rita Mancini[5]

To cite: Bruschini S, Pallocca M, Sperandio E, *et al*. Deconvolution of malignant pleural effusions immune landscape unravels a novel macrophage signature associated with worse clinical outcome in lung adenocarcinoma patients. *Journal for ImmunoTherapy of Cancer* 2022;**10**:e004239. doi:10.1136/jitc-2021-004239

► Additional supplemental material is published online only. To view, please visit the journal online (http://dx.doi.org/10.1136/jitc-2021-004239).

SB and MP contributed equally.

SB and MP are joint first authors.

Accepted 27 April 2022

For numbered affiliations see end of article.

Correspondence to
Dr Gennaro Ciliberto;
gennaro.ciliberto@ifo.it

ABSTRACT

Background Immune checkpoint inhibitors are still unable to provide clinical benefit to the large majority of non-small cell lung cancer (NSCLC) patients. A deeper characterization of the tumor immune microenvironment (TIME) is expected to shed light on the mechanisms of cancer immune evasion and resistance to immunotherapy. Here, we exploited malignant pleural effusions (MPEs) from lung adenocarcinoma (LUAD) patients as a model system to decipher TIME in metastatic NSCLC.

Methods Mononuclear cells from MPEs (PEMC) and peripheral blood (PBMC), cell free pleural fluid and/or plasma were collected from a total of 24 LUAD patients and 12 healthy donors. Bulk-RNA sequencing was performed on total RNA extracted from PEMC and matched PBMC. The DEseq2 Bioconductor package was used to perform differential expression analysis and CIBERSORTx for the regression-based immune deconvolution of bulk gene expression data. Cytokinome analysis of cell-free pleural fluid and plasma samples was performed using a 48-Plex Assay panel. THP-1 monocytic cells were used to assess macrophage polarization. Survival analyses on NSCLC patients were performed using KM Plotter (LUAD, N=672; lung squamous cell carcinoma, N=271).

Results Transcriptomic analysis of immune cells and cytokinome analysis of soluble factors in the pleural fluid depicted MPEs as a metastatic niche in which all the components required for an effective antitumor response are present, but conscripted in a wound-healing, proinflammatory and tumor-supportive mode. The bioinformatic deconvolution analysis revealed an immune landscape dominated by myeloid subsets with the prevalence of monocytes, protumoral macrophages and activated mast cells. Focusing on macrophages we identified an MPEs-distinctive signature associated with worse clinical outcome in LUAD patients.

Conclusions Our study reports for the first time a wide characterization of MPEs LUAD microenvironment, highlighting the importance of specific components of the myeloid compartment and opens new perspectives for the rational design of new therapies for metastatic NSCLC.

WHAT IS ALREADY KNOWN ON THIS TOPIC

⇒ Tumor immune microenvironment (TIME) is a key element in determining resistance to immunotherapy with immune checkpoint inhibitors. Malignant pleural effusions (MPEs), a pathological condition associated with 30% of non-small cell lung cancer cases, represent an easily accessible window onto metastatic disease.

WHAT THIS STUDY ADDS

⇒ By using MPEs and blood samples directly derived from lung adenocarcinoma (LUAD) patients and exploiting cytokinome analysis and transcriptomic data combined with an immune deconvolution-based approach, we provide a deep characterization of cellular and soluble components of MPEs microenvironment. The main novelty of our findings relies in the identification in MPEs of a cytokinome fuelling monocytes infiltration and protumoral Macrophage (Mφ) polarization and of a novel Mφ genes signature associated with poor prognosis in LUAD.

HOW THIS STUDY MIGHT AFFECT RESEARCH, PRACTICE AND/OR POLICY

⇒ This study highlights the involvement of the myeloid compartment in the context of LUAD TIME and provides a solid ground for the identification of new targets for the treatment of metastatic disease.

INTRODUCTION

Immunotherapy is revolutionizing the clinical management of non-small cell lung cancer (NSCLC), mainly through the introduction of immune checkpoint inhibitors (ICIs).[1 2] However, despite previously unanticipated long-term responses in advanced disease have been obtained in a subset of patients, the main hurdle remains the lack of efficacy in the vast majority of cases.[3 4] Several resistance mechanisms to immunotherapy have been identified, involving tumor cell intrinsic as well as tumor cell-extrinsic factors.[5] The latter can be mainly ascribed to components of the tumor microenvironment (TME).[6] Although the main efforts have been devoted to T-cell characterizations with the development of ICI therapies, other immune cells of the innate and adaptive immune systems, including DCs, macrophages, NK cells, and B cells, have also been shown to contribute to tumor progression and response to immunotherapy.[7 8] Hence, a comprehensive characterization of the tumor immune microenvironment (TIME) is essential.[9] In this regard recently a detailed immune cell atlas of early-stage lung cancer has provided novel insights into the functional states and developmental lineages of heterogeneous myeloid subsets.[10] An exemplary proof of myeloid complexity is given by the macrophage compartment. It is well known nowadays that tumor-associated macrophages (TAMs) are highly plastic cells and have a pivotal role in shaping the TME and response to therapy.[11] Moreover, high infiltration of TAMs is associated with poor overall survival in different tumor types,[12] making them an important target for cancer treatment.[13 14] Nevertheless, the lack of complete understanding of molecular and functional diversity of the tumor macrophage compartment strongly limits therapeutic approaches. Very recently, focusing on how different macrophage lineages contribute to TME and cancer progression, tissue-resident macrophages have been proposed as target for prevention and treatment of early NSCLC.[15] However, currently the majority of NSCLC cases are diagnosed at an advanced stage, and approximately 30% present the development of malignant pleural effusion (MPEs), a pathological condition mostly associated with poor prognosis.[16 17] Even if in the last years several studies reported a thorough characterization of tumor heterogeneity and TME landscape of lung cancer from early to advanced stages,[10 18–20] a real focus on metastatic sites was not yet provided.

MPEs, that arise when metastatic cancer cells infiltrate thoracic lymph nodes as well as the pleura, result in the accumulation of a fluid in which cancer and immune cells, stroma and their soluble factors interact promoting tumor proliferation, epithelial-mesenchymal transition and the emergence of most aggressive neoplastic cells.[21–24] In this view MPEs, that are routinely therapeutically drained, represent an easily accessible and little invasive approach to investigate the types of interactions that occur in the TME of advanced lung cancer. In past years, our group has reported that MPEs from lung adenocarcinoma (LUAD) patients are a valuable source of primary tumor cells, that show stem-like features when cultured in three-dimensional conditions.[25–27] In this study, we exploited MPEs from LUAD patients as a model system to investigate the TME of metastatic NSCLC.

METHODS

Human specimens

MPEs and blood samples were obtained from 24 patients with histologically or cytologically confirmed diagnosis of LUAD complicated with MPEs. Patients were enrolled from three different medical centers in Rome, Istituti Fisoterapici Ospedalieri, Sant'Andrea Hospital and Policlinico Umberto I (Sapienza University of Rome) and named respectively as BBIRE, SA and PUC followed by a progressive patient number. Twenty-four patients consisted of 9 males and 15 females with a median of 66 years old. Blood samples from 12 healthy donors (HDs) were also collected (median age of 62 years old). Additional information regarding the clinical history of subjects involved in the study are reported in online supplemental table S1.

Mononuclear cell from pleural effusions and peripheral blood isolation from LUAD patients and HD

Mononuclear cell from pleural effusions (PEMC) and peripheral blood (PBMC) of LUAD patients and HD were isolated via OncoQuick (Greiner Bio-One) and Lympholyte-H (Cedarlane, Ontario, California, USA) gradient separation media. More details on samples processing are reported in online supplemental methods.

Quantitative real-time PCR analysis

Quantitative real-time PCR (qRT-PCR) was performed as previously described.[28] TaqMan probes for CCL3, CCL20, CXCL2, IL6, VEGFA and GAPDH were purchased from Applied Biosystems. Primers used for individual genes were previously reported,[29] except for β-actin: Fw (5'–3')-GCCGGGACCTGACTGACT; Rv (5'–3')-TGGTGATGACCTGGCCGT. The mRNA levels were normalized using β-actin or GAPDH, as specified. The two housekeeping genes present similar expression levels among the various groups.

Bulk RNA Sequencing

Total RNA was extracted from PEMC and matched PBMC of five LUAD patients and from PBMC of four HDs, using Qiazol (Qiagen, Hilden,Germany), purified from DNA contamination through a DNase I (Qiagen) digestion step, and further enriched by Qiagen miRNeasy columns profiling (Qiagen). Quantity and integrity of the extracted RNA were assessed by Nanodrop Spectrophotometer (Nanodrop Technologies, Thermofisher, Waltham, Massachusetts, USA) and by Agilent 2100 Bioanalyzer (Agilent Technologies, Santa Clara, California, USA), respectively. RNA libraries preparation, sequencing and subsequent bioinformatic analyses are described in online supplemental methods. RNA-seq

derived visualizations were generated via the AUTO-go framework.[30]

CIBERSORTx deconvolution analysis

To determine the proportion of 22 different immune cell types in each sample, the gene expression data, obtained by RNA-seq, were uploaded to the CIBERSORTx webtool[31] (https://cibersortx.stanford.edu/). The algorithm was run using the LM22 signature matrix, that defines 22 infiltrating immune populations based on the expression of 547 different genes, for 1000 permutations. We used bulk-mode batch correction and the output was in absolute mode, that reflects the absolute proportion of each cell type in the mixture. Only cases with a CIBERSORTx output p<0.05 were chosen for further analysis. Then, the estimated cell type abundances were used to realize a differential deconvolution analysis by applying a paired or unpaired Student's t-test between the immune cell populations for the groups of interest.

Statistical analysis

Statistical analyses were performed using GraphPad Prism V.8.0 software and R environment for statistical computing (V.4.1.0). Groups were compared by Student's t-test or Wilcoxon signed-rank test as indicated and statistical significance is represented in figures as follows: *p<0.05; **p<0.01; ***p<0.001 and ****p<0.0001.

RESULTS

Transcriptional profiling of LUAD PEMC and PBMC reveals an immunosuppressive and tumor-promoting TIME in LUAD pleural effusions

An overview of the workflow followed in the study is schematically represented in figure 1. First, we performed a bulk RNA Sequencing (RNA-seq) on immune mononuclear cells isolated from MPEs (PEMC) and peripheral blood (PBMC) of five LUAD patients and on PBMC from a group of four HDs, as control. More detailed information on patients' characteristics and HDs enrolled are reported in online supplemental table S1.

Principal component analysis (PCA) and hierarchical clustering clearly segregated the transcriptomic profiles of the three different groups (figure 2A,B). This suggests that not only PEMC and PBMC from the

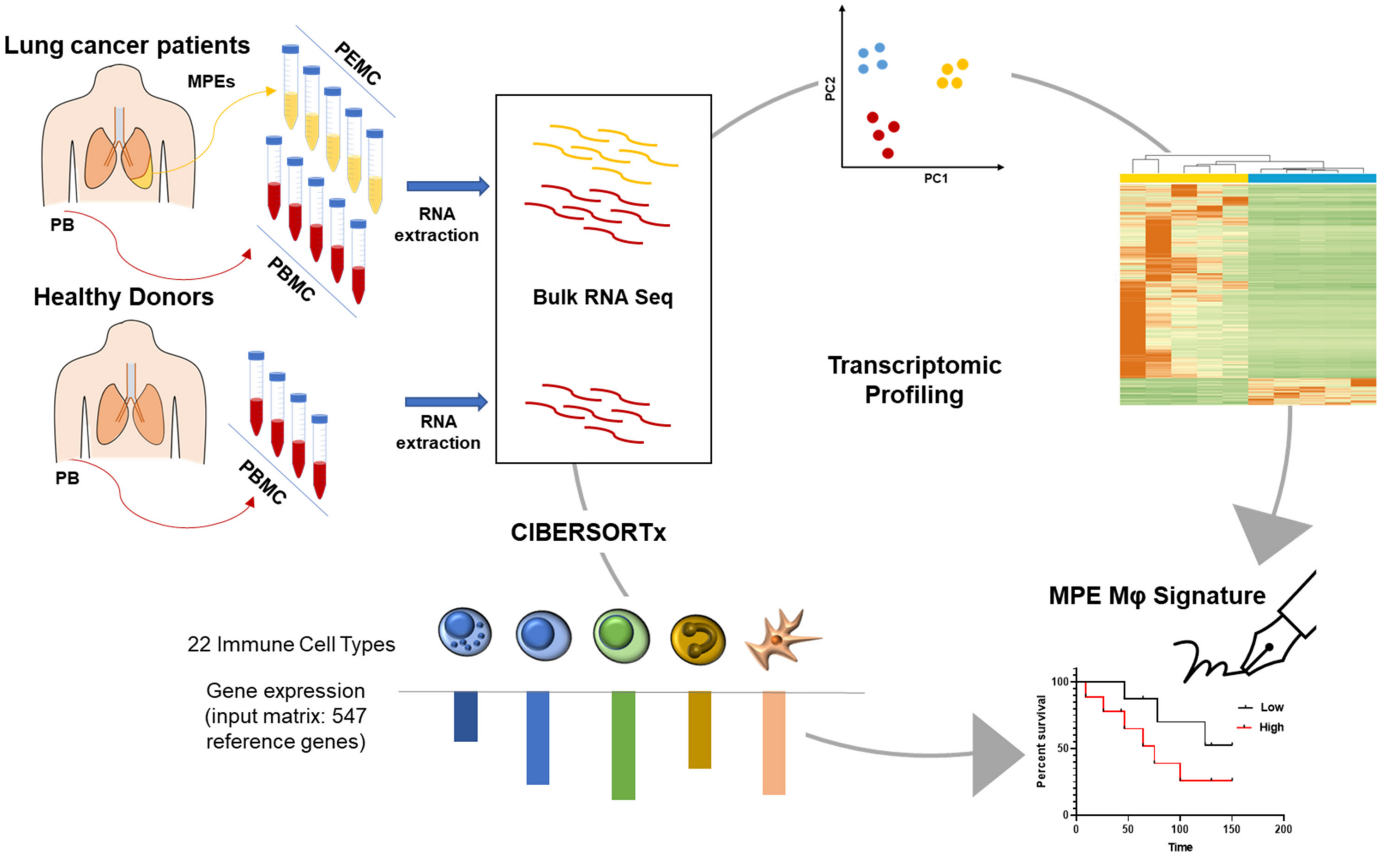

Figure 1 Schematic overview of the experimental workflow followed in the study. First, RNA from PEMC and matched PBMC of five LUAD patients and PBMC of four HD was extracted to perform a bulk RNA-Seq. PCA and DEA were performed to define the transcriptomic profile of LUAD immune cells and highlight differences between samples. Afterwards, to infer the immune cell proportions in each sample, RNA Seq data were subjected to CIBERSORTx deconvolution analysis. The tool permits to quantify at once the abundance of 22 immune cell types, based on a 547 genes signature matrix (LM22). Finally, this combined approach also allowed us to identify an MPEs macrophage (MPEs Mϕ) signature related to patients' clinical outcome. DEA, differential expression analysis; HD, healthy donors; LUAD, lung adenocarcinom; PCA, principal component analysis; PBMC, peripheral blood mononuclear cells; PEMC, pleural effusion mononuclear cells

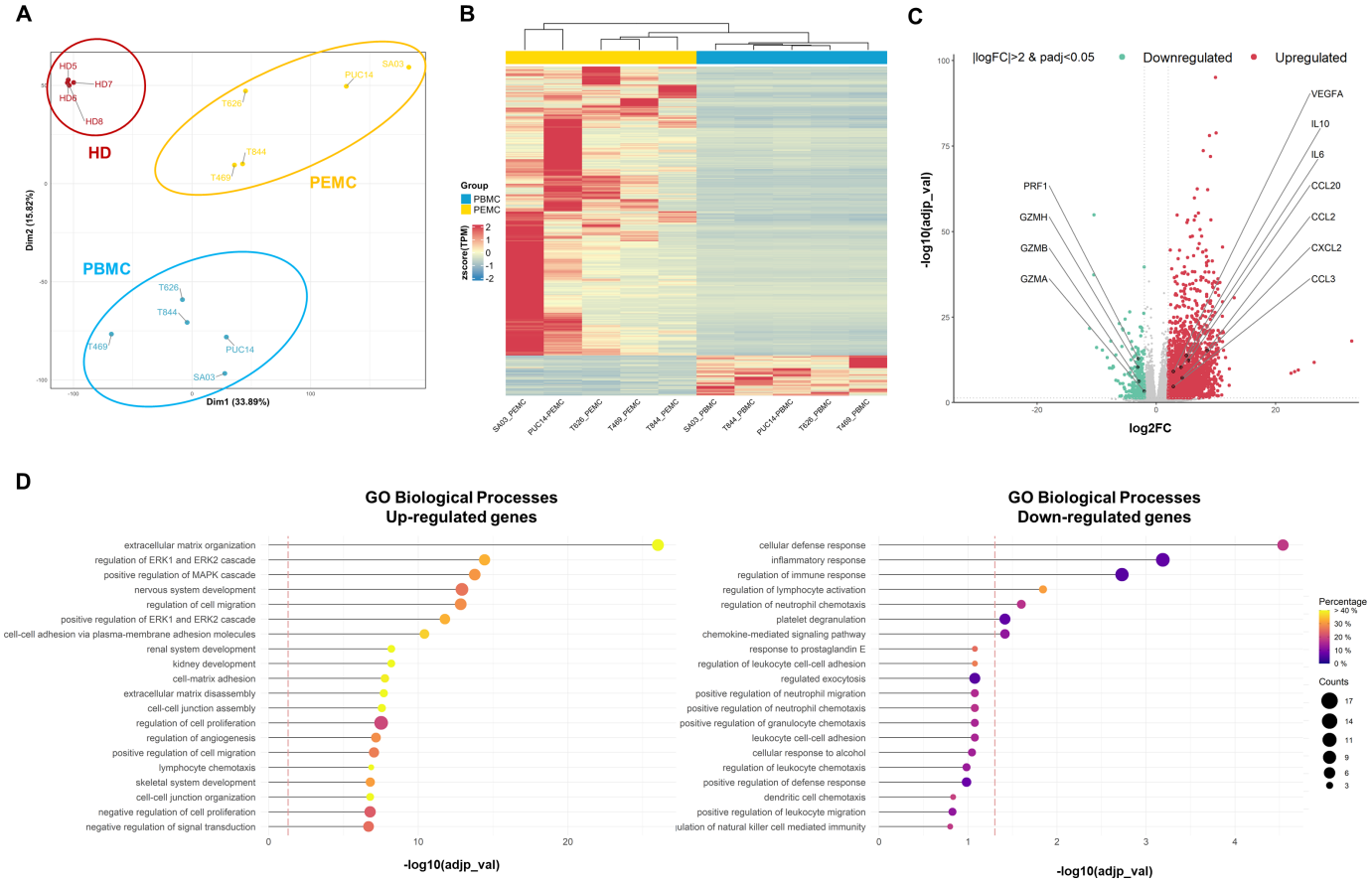

Figure 2 Transcriptional profiling of LUAD PEMC and PBMC reveals an immunosuppressive and tumor-promoting TIME in LUAD Pleural Effusions. (A) Principal component analysis performed on PEMC (yellow dots, n=5) and PBMC (blue dots, n=5) of LUAD patients and PBMC of HD (red dots, n=4) transcriptome. (B) Hierarchical clustering of all DEGs between LUAD PEMC and matched PBMC. Expression values are Z score transformed. Samples were clustered using complete linkage and Euclidean distance. (C) Volcano plot showing upregulated (red dots) and downregulated genes (green dots) resulted from the differential expression analysis performed on LUAD PEMC versus PBMC. Only genes with |Log2FC|>2 and adjp_val<0.05 were considered significantly deregulated. Some of the most relevant genes are reported. (D) Gene ontology (GO) analysis of upregulated genes (left panel) and downregulated genes (right panel) in PEMC versus PBMC of LUAD patients. Terms over red dashed line are considered statistically significant (adjp_val<0.05). adjp_val, adjusted p_value; DEGs, differentially expressed genes; FC, fold change; HD, healthy donor; LUAD, lung adenocarcinoma; PEMC, pleural effusion mononuclear cell.

same patients are transcriptionally distinct, as in part expected given their different origin, but also that PBMC from LUAD patients are substantially transcriptionally different from those of HDs (online supplemental files 3; 4).

Differential expression analysis (DEA) revealed 2694 differentially expressed genes (DEGs) in PEMC compared with their matched PBMC (2363 upregulated and 331 downregulated; |Log2Fold Change|>2 and adjusted p<0.05, online supplemental table S2A) (figure 2C) and 1275 DEGs in LUAD vs HD PBMC (834 upregulated and 441 downregulated; |Log2Fold Change|>2 and adjusted p<0.05, online supplemental table S2B and figure S1B).

The functional gene ontology (GO) enrichment analysis performed on the DEGs resulting from LUAD versus HD PBMC comparison, revealed, with respect to biological processes (BP), a set of enriched terms such as cellular response to cytokine stimulus, inflammatory response, positive regulation of cell migration and angiogenesis for the downregulated genes in patients' PBMCs and no significant enriched term for the upregulated ones (online supplemental figure S1C and table S3A,B). This could suggest a certain level of dormancy of circulating immune cells in LUAD patients with respect to HDs.

Most importantly, the GO BP enrichment analysis performed on DEGs in PEMC with respect to their matched PBMC revealed a number of enriched terms related to tumor promotion for the upregulated genes, such as cell migration, extracellular matrix organization, angiogenesis, cellular proliferation, and a set of terms related to immune response for the downregulated genes (figure 2D and online supplemental table S3C,D).

Based on this analysis, we selected a set of DEGs more representative of this tumor-promoting and immune suppressive phenotype and split them into three main clusters: growth factors and metastatic/angiogenic promoters, inflammatory chemokines, and cytokines/

enzymes related to regulation of immune response (online supplemental figure S2A). qRT-PCR analysis performed on the RNA-Seq cohort and on nine additional LUAD patients (online supplemental table S1) confirmed a significantly increased expression of some of these proinflammatory cytokines and chemokines genes such as CXCL2, CCL20, IL6 and VEGFA in PEMC compared with matched LUAD PBMC (online supplemental figure S2B). The same validation performed on LUAD and HD PBMC confirmed the downregulation of CXCL2, CCL20 and VEGFA in LUAD patients respect to HDs (online supplemental figure S1D). Overall, these data suggest that in the microenvironment of MPEs immune cells acquire, with respect to their circulating counterpart (ie,PBMC), an immunosuppressive and tumor-promoting profile.

Deconvolution of bulk gene expression data depicts the Immune Landscape of LUAD MPEs and underpins the importance of myeloid compartment

In order to define the immune cell landscape of MPEs, the next step was to perform a deconvolution analysis of the gene expression data obtained from the RNA-Seq, described in the previous paragraph, exploiting CIBERSORTx, a tool which uses predefined immune cells specific gene signature matrices for the in silico quantification of 22 different immune types.[31] Algorithm execution allowed us to infer the immune composition of our samples (online supplemental table S1) reported both as absolute score (see heatmap figure 3A and online supplemental table S4A), and as estimated relative fractions (see bar plot figure 3B). These data clearly show how samples belonging to each group cluster together, demonstrating that there are strong differences in the immune cell composition among the three groups. Moreover, samples belonging to each group show a similar immune landscape, even if, similar to the observations in other studies,[18–20] a certain variability among patients' samples is appreciable and most pronounced in the PEMC group. Of note, the four HD PBMC samples show a very homogeneous and reproducible immune pattern, thus confirming the robustness of the deconvolution analysis. The analysis revealed that out of the detectable 22 immune cell types, each deconvoluted group contains a variety of them ranging from 11 in HD PBMC to 15 in LUAD PBMC and

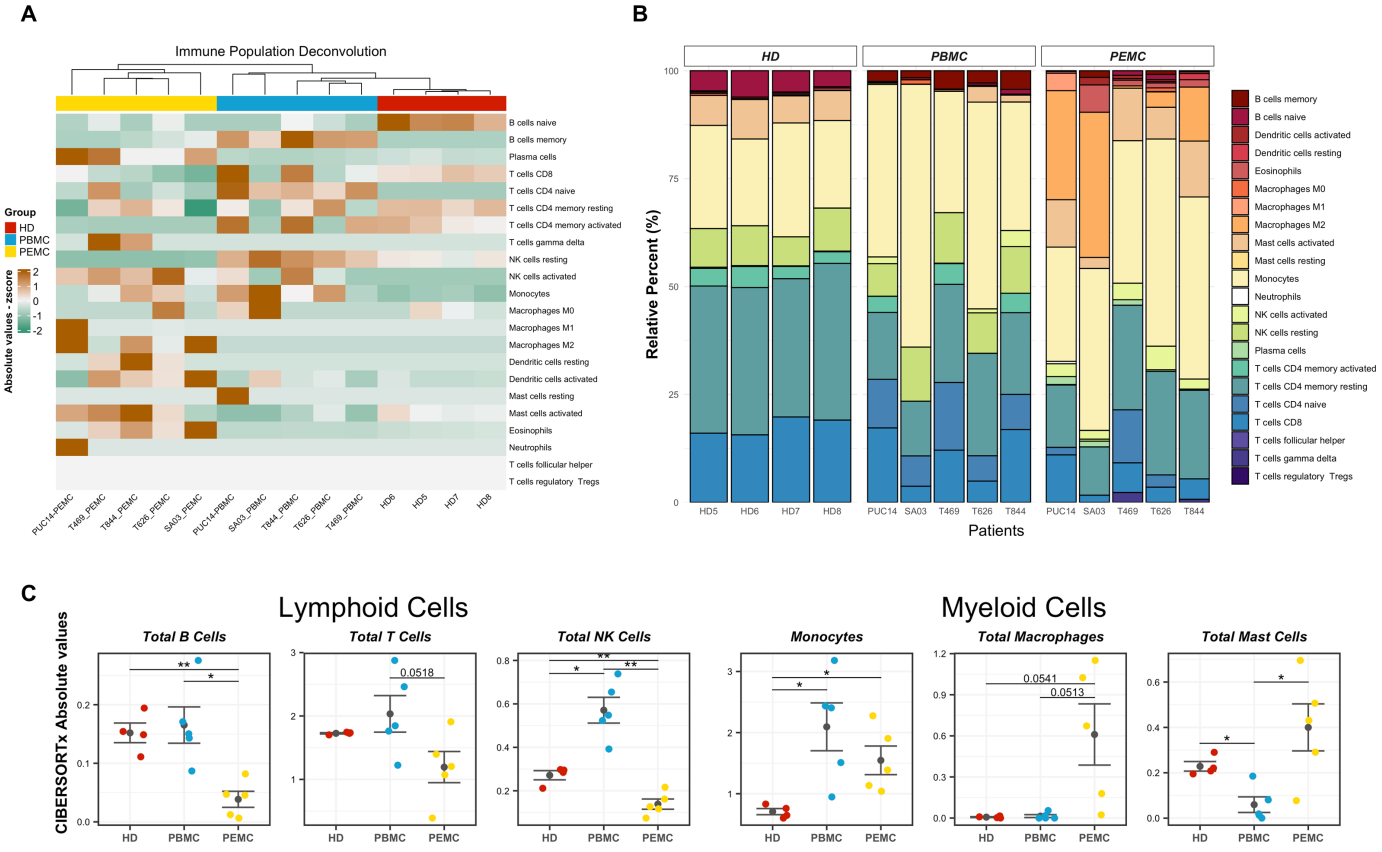

Figure 3 CIBERSORTx deconvolution analysis depicts the Immune Landscape of LUAD MPEs. (A) Heatmap showing the absolute abundances of 22 immune cell types in each sample. Hierarchical clustering shows a clear segregation of the samples according to their originating group, LUAD PEMC (yellow), LUAD PBMC (blue) and HD PBMC (red). Absolute values are Z score transformed. (B) Stacked bar plots reporting the estimated relative fractions of each immune cell type in a given mixture sample. (C) Dot plots showing the comparisons of total lymphoid and myeloid immune cells between the three sample groups. Each dot represents one patient. Mean values and SD for each cell subset were calculated for each patient group and compared using paired (LUAD PEMC vs PBMC) or unpaired (LUAD PBMC *vs* HD) two-tailed Student's t-test. *P<0.05; **p<0.01. HD, healthy donor; LUAD, lung adenocarcinoma; PBMC, peripheral blood mononuclear cells; PEMC, pleural effusion mononuclear cells.

19 in LUAD PEMC. Only follicular helper T cells and regulatory T cells (Tregs) were not found in any group. Instead, both eosinophils and neutrophils were detected in a very low proportions and the latter only in one PEMC sample (figure 3A,B and online supplemental table S4A). Regarding the immune cell distribution in HD PBMC the most abundant populations are represented by CD4 T cells (mainly CD4 memory resting), followed by monocytes and CD8 T cells (roughly in a 2:1 ratio with CD4 T cells) with a smaller fractions of NK cells resting, activated mast cells, naïve B cells and a very small fraction of activated dendritic cells (DCs) (figure 3B,C, online supplemental figure S3). These results are completely in line with the well-known relative abundancies of immune cell populations found in normal human blood samples,[32] underpinning the reliability of this in silico approach.

Looking at the immune composition of LUAD PBMC, even if the overall proportion between immune cell types is conserved with respect to that of HD PBMC, some differences can be identified, as shown by the differential deconvolution analysis (online supplemental table S4B). T CD4 cells remain the most abundant lymphocytes. However, respect to HD it is possible to detect not only CD4 memory resting and activated ones, but also naïve CD4 T cells. The total proportion of B cells is also conserved with a switch from naïve B cells to memory ones. Instead, an increased fraction of NK cells is observed with the appearance also of activated NK, even if in a 1:10 ratio with NK resting cells. Furthermore, a strong decrease in activated mast cells is appreciable. Most importantly, in LUAD PBMC the most abundant cell type is represented by monocytes and not anymore by CD4 T cells (figure 3B,C, online supplemental figure S3). Of note, this finding is in line with the upregulation in LUAD versus HD PBMC of the most relevant receptors involved in monocytes migration and macrophage differentiation,[33 34] such as CCR2, CX3CR1 and CSF1R, as shown by DEA performed on RNA-seq data (online supplemental figure S1B).

We used these results as a baseline of the immune status in LUAD patients to unravel the specific features of the MPEs immune landscape. When we looked at immune cell composition of LUAD PEMC we found that, as in LUAD PBMC, the two most abundant immune cell types are represented by monocytes and CD4 T cells. However, the differential deconvolution analysis (online supplemental table S4B) showed a decreasing trend in the overall content of all effector cells, such as total T and B lymphocytes and NK cells in PEMC compared with PBMC (figure 3C). With respect to CD4 T cells the main difference was found in CD4 T activated memory cells. The same trend was observed in CD8 T cells, even if statistical significance was not reached. There is also an overall decrease in B cells content with a significant switch from memory B cells to plasma cells. Of note, even if a small fraction of NK activated cells is detectable there is a clear decrease in the overall content of NK cells (figure 3C and online supplemental figure S3). As in PBMC a very small fraction of activated DC cells is detectable, with the appearance of a comparable fraction of resting DC in three out of five patients (figure 3A and online supplemental figure S3). Most importantly, in MPE compartment the high proportion of monocytes is supported by a prominent increase of protumoral M2 polarized macrophages and activated mast cells (figure 3C and online supplemental figure S3). This is in line with the immunosuppressive and tumor promoting profiling of PEMC that we defined by DEA (figure 2C,D). Overall, these results depict a TIME in which both adaptative and innate immune cells are still present but dominated by monocytes/protumoral M2 macrophages, that in concert with activated mast cells, could sculpt the TIME toward an immunosuppressive phenotype.

Since the enrichment of M2 macrophages in LUAD PEMC respect to PBMC is very pronounced, but borderline for statistical significance (p=0.0528), to validate these results, we assessed by qRT-PCR the mRNA expression levels of M2 (ie, CD163, IL10, CD206 and CCL22) and M1 (ie, COX-2, IL1B and IL12) specific macrophage markers in PEMC and matched PBMC of the RNA-Seq cohort and nine additional LUAD patients. The analysis confirmed a significantly upregulation of the M2 markers in PEMC. Instead, no significant variations were detected for the M1 markers (figure 4A). The same analysis performed on LUAD and HD PBMC revealed no clear polarization toward M1 or M2 phenotypes (figure 4B).

Finally, to further strengthen the concept that, in the microenvironment of MPEs, monocytes are induced to acquire a protumoral M2 phenotype, THP1-derived macrophages were stimulated for 48 hours with serum free medium (M0 macrophages) or medium supplemented with cell-free MPE material from LUAD patients (figure 4C). qRT-PCR evaluation of M1/M2 markers clearly showed that MPEs from three different patients, included in the RNA-seq experiment, induced a marked and significant increase of three M2 genes (CD163, IL10 and CD206) and a parallel decrease of two M1 genes (IL1B and IL12) when compared with the baseline mRNA levels of M0 macrophages (figure 4D), thus confirming the M2-polarizing activity of MPEs.

Cytokinome analysis of LUAD MPEs confirms an immunosuppressive, wound healing and tumor promoting environment

The bioinformatic analysis described in previous paragraphs revealed a proinflammatory, immunosuppressive and tumor promoting profile of the cellular component in the TIME of MPEs. Since soluble factors are known to play a pivotal role in shaping the TME, the levels of 48 different cytokines and growth factors were evaluated in MPEs-derived cell free supernatant and plasma of 15 different LUAD patients and of 4 HDs, as control (online supplemental table S5A). PCA and hierarchical clustering show that MPEs and plasma of LUAD patients are characterized by distinctive cytokine patterns that could, in part, explain the differential immune cell composition in these two compartments. Instead, a similar cytokine pattern

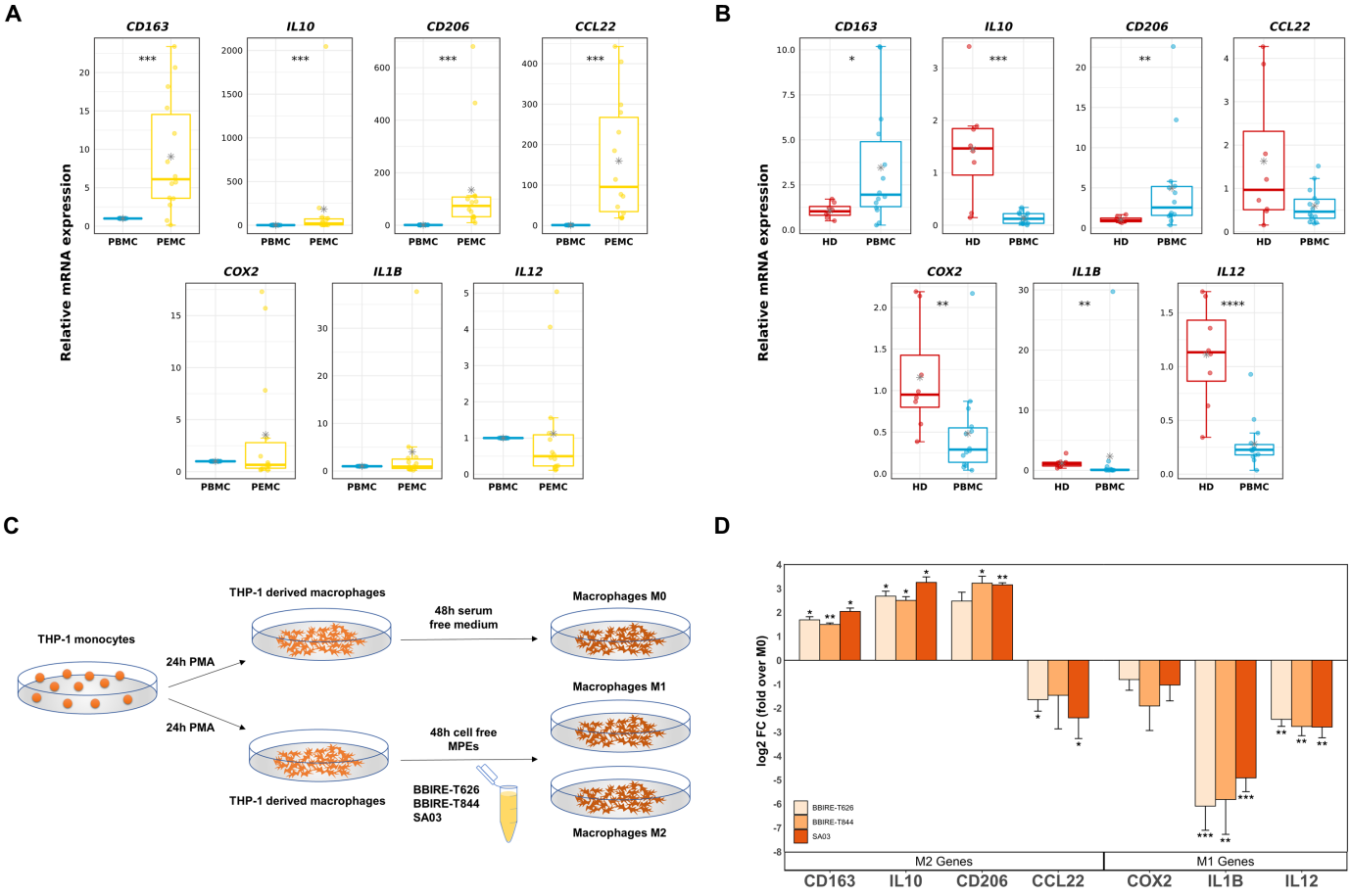

Figure 4 In the immune contexture of MPEs macrophages acquired a protumoral M2 phenotype. Quantitative real-time PCR (qRT-PCR) analyses showing the mRNA levels of M2 (CD163, IL10, CD206, CCL22) and M1 (COX2, IL1B, IL12) specific marker genes in LUAD PEMC compared with matched PBMC (A) and in LUAD PBMC compared with HD PBMC (B). β-actin was used as housekeeping gene. The box plot represents minimum and maximum values (whiskers), median values (center lines), mean values (center aterisk) and 25th and 75th percentiles (box edges), with all data points plotted. Each dot represents one patient (healthy: n=8; patients: n=14). *P<0.05, **p<0.01, ***p<0.001, ****p<0.0001 (Wilcoxon signed-rank test). (C) Schematic representation of THP-1 in vitro differentiation and macrophage polarization. THP1 monocytes were differentiated into macrophages in the presence of PMA (phorbol-12-myristate-13-acetate) and then stimulated with serum free medium (M0 macrophages) or with medium supplemented with 10% of cell-free pleural effusion material from three different LUAD patients (BBIRE-T626, BBIRE-T844 and SA03). After 48 hours, macrophage polarization was assessed by qRT-PCR evaluation of the mRNA levels of M1/M2-specific marker genes. (D) qRT-PCR analysis of M2 and M1 marker genes in THP-1 cells after 48 hours exposure to serum free medium (M0 macrophages) or medium supplemented with MPEs supernatant from LUAD patients. Data are reported as log2FC of the mRNA levels in treated THP1 over M0 macrophages (β-actin was used as housekeeping gene). The mean±SEM of three independent experiments is reported. *P<0.05, **p<0.01, ***p<0.001 (two-tailed Student's t-test). HD, healthy donor; LUAD, lung adenocarcinoma; MPEs, malignant pleural effusions; PBMC, peripheral blood mononuclear cells; PEMC, pleural effusion mononuclear cells.

was observed in LUAD and HD plasma (figure 5A,B), suggesting that the main differences between patients and HDs do not reside in the soluble component. Based on this result, we focused our attention on LUAD patients and sought to define the characteristic cytokine profile of MPEs. To this purpose we (1) clustered the cytokines based on their concentration, ranging from <5 pg/mL up to 80 ng/mL (figure 5C); (2) calculated the fold increase or decrease of MPEs cytokines with respect to their systemic levels (ie, plasma of matched LUAD patients). As reported in table 1, 29 out of the 48 cytokines analyzed resulted statistically different between the two groups of samples. Fewer differences were observed for LUAD/HDs comparison with increased levels of some cytokines, such as IL-6, IL-8, VEGFA and IL-2ra, in patients' plasma respect to that of HDs, as also previously reported[35] (online supplemental figure S4 and table S5B).

Focusing on LUAD plasma/MPEs comparison, even if SCGF-b represents the most concentrated cytokine in MPEs (83,287.1±8944 pg/mL in LUAD MPEs vs 25,082.5±3814 pg/mL in LUAD plasma), IL-6 shows a very high discrepancy between pleural fluid and plasma of LUAD patients (fold=413.9). Based on both parameters, it was possible to highlight different classes of cytokines that shape the MPEs microenvironment: (1) proinflammatory cytokines (ie, IL6, IL8, and CCL2); (2)

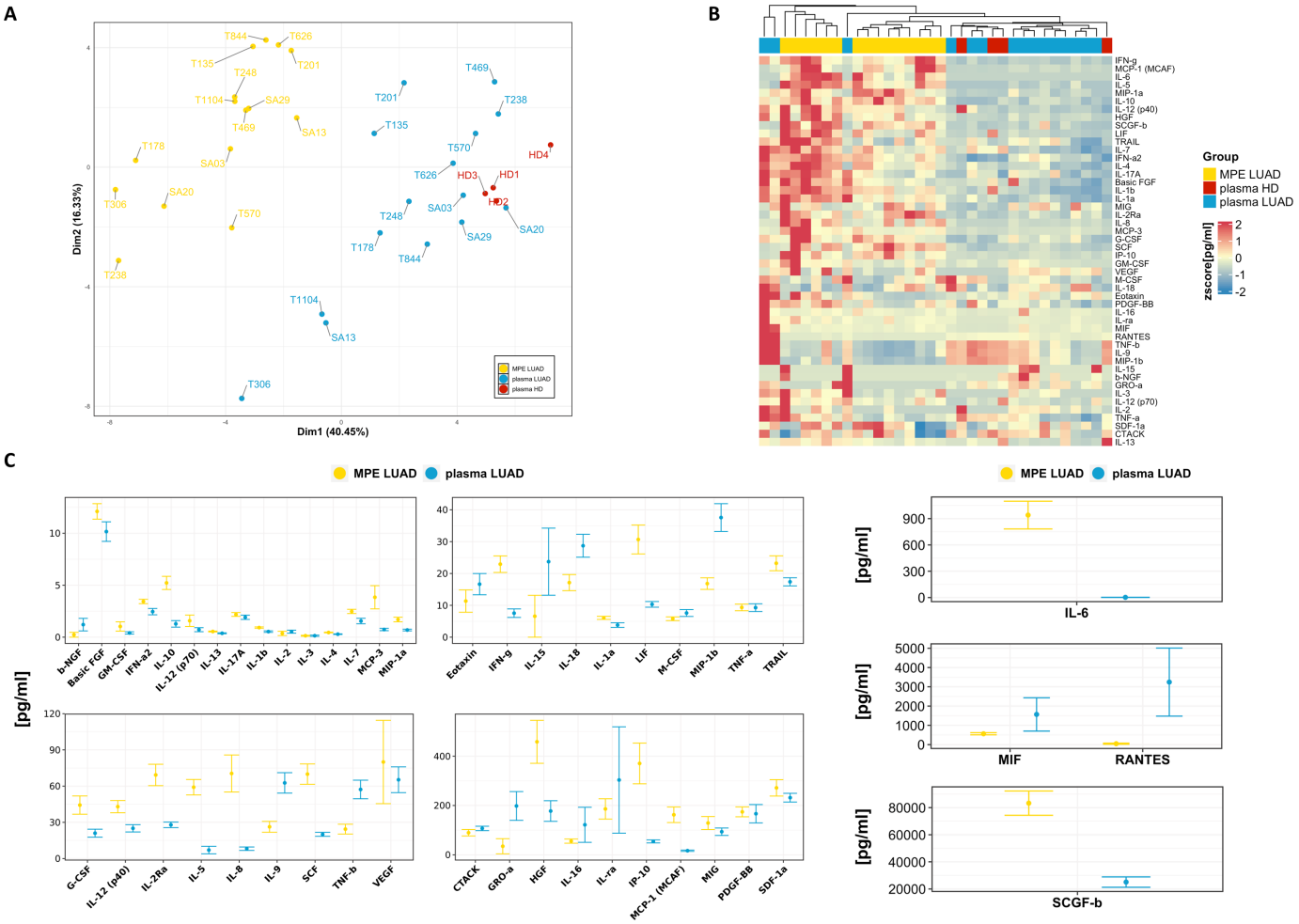

Figure 5 Cytokinome analysis of LUAD MPEs confirms an immunosuppressive, wound healing and tumor promoting environment. Principal component analysis (A) and hierarchical clustering (B) of 48 different cytokines levels evaluated in cell free pleural fluid and plasma of 15 LUAD patients (yellow and blue, respectively) and plasma of 4 HD (red) using a Bio-Plex sandwich immunoassay (see online supplemental methods). (C) Scatter plots showing the mean values±SEM (n=15) of cytokines concentration (pg/mL), evaluated in MPE and plasma of 15 LUAD patients. HD, healthy donor; LUAD, lung adenocarcinoma; MPE, malignant pleural effusion.

cytokines and growth factors linked to the maintenance of a stem like tumor phenotype (ie, IL6, IL8, SCF, SCF-b, LIF, and HGF)[36 37]; (3) cytokines that promote monocytes infiltration and Th2/M2 polarization (ie, IL6,CCL2, IL5, IL10, and MCP-3),[34 38 39] even if the lasts with medium and low concentration (table 1), but with high fold increase respect to plasma, suggesting a specific role in MPEs microenvironment. Furthermore a nascent but thwarted effector response in LUAD MPEs is witnessed by (1) the high concentration of CXCL10, a chemokine well known to play a role in T cell trafficking and activation,[40] in line with the high proportion of CD4 T cells in LUAD PEMC, as shown by our deconvolution analysis; (2) the presence of effector cytokines (ie, INFα2, MIP1α, INFγ, and TNFβ) in a relatively low levels, but significantly higher with respect to plasma (excepted for TNFβ). These results suggest that soluble factors identified in the microenvironment of MPEs contribute to the creation of a proinflammatory and immunosuppressive environment that probably shape the immune cellular component from an effector toward an inactive mode. Moreover, wound healing assays, performed on two MPEs-derived primary cell lines stimulated for 24 hours with their matched cell free MPE supernatant, clearly show how these soluble components also impact onto tumor migratory capacity in the MPEs microenvironment (online supplemental figure S5).

A novel MPE-associated gene signature correlates with poor prognosis in LUAD patients

All our previous observations suggested the involvement of macrophages in the immune contexture of LUAD MPEs, where they acquire a protumoral M2 phenotype.

Two ontologically different macrophage types are known to populate adult lungs: tissue resident macrophages (TRMs) and monocytes derived macrophages (MDMs). To analyze the components that populate MPEs we tested the expression of a TRM and an MDM signature, identified in early-stage human NSCLC lesions,[15] in our RNA Seq data from LUAD PEMC and PBMC.

Table 1 List of 29 cytokines differentially expressed between cell free pleural fluid and plasma of LUAD patients

	MPEs concentration (pg/mL)	Plasma concentration (pg/mL)	Fold MPEs/plasma	P value
SCGF-b	83 287.1 (±8944)	25 082.5 (±3814)	3.3	<0.0001
IL-6	940.1 (±158.3)	2.3 (±0.9)	413.9	<0.0001
HGF	458.1 (±87.1)	177.5 (±41.8)	2.6	0.0205
IP-10 (CXCL10)	370.5 (±82.6)	54.3 (±6.1)	6.8	0.0018
MCP-1 (CCL2)	162.3 (±31.4)	16.6 (±2.7)	9.8	0.0005
IL-8	70.5 (±15.3)	8.2 (±3.1)	8.6	0.0008
SCF	70.0 (±8.4)	20.1 (±1.7)	3.5	<0.0001
IL-2Ra	69.2 (±8.9)	27.9 (±2.3)	2.5	0.0001
IL-5	59.1 (±6.4)	7.0 (±3.1)	8.4	<0.0001
G-CSF	44.3 (±7.6)	21.0 (±3.3)	2.1	0.0021
IL-12 (p40)	43.0 (±5.1)	25.0 (±3.0)	1.7	0.0200
GRO-a (CXCL1)	34.7 (±30.7)	198.1 (±58.4)	0.2	0.0355
LIF	30.7 (±4.5)	10.3 (±0.9)	3.0	0.0008
IL-9	26.3 (±4.5)	62.7 (±8.5)	0.4	0.0022
TNF-b	24.4 (±4.1)	57.2 (±7.7)	0.4	0.0023
TRAIL	23.2 (±2.3)	17.4 (±1.3)	1.3	0.0363
IFN-g	22.9 (±2.6)	7.5 (±1.3)	3.0	<0.0001
IL-18	17.1 (±2.5)	28.7 (±3.6)	0.6	0.0282
MIP-1b (CCL4)	16.8 (±1.8)	37.6 (±4.4)	0.4	0.0008
IL-1a	6.1 (±0.5)	3.8 (±0.7)	1.6	0.0278
M-CSF	5.8 (±0.6)	7.6 (±1.1)	0.8	0.0274
IL-10	5.2 (±0.6)	1.3 (±0.3)	4.1	0.0002
MCP-3 (CCL7)	3.8 (±1.1)	0.7 (±0.1)	5.2	0.0132
IFN-a2	3.4 (±0.2)	2.5 (±0.3)	1.4	0.0284
IL-7	2.5 (±0.2)	1.6 (±0.3)	1.6	0.0008
MIP-1a (CCL3)	1.7 (±0.2)	0.7 (±0.1)	2.5	0.0001
IL-1b	0.9 (±0.1)	0.5 (±0.1)	1.7	0.0015
IL-13	0.5 (±0.04)	0.4 (±0.05)	1.5	0.0026
IL-4	0.5 (±0.03)	0.3 (±0.03)	1.6	0.0006

Cytokines are listed based on the higher concentration in MPEs. Mean values of concentration ±SEM (n=15) are reported for each cytokine in each group. Fold is considered statistically significant if p<0.05 (two-tailed Student's t-test).
LUAD, lung adenocarcinoma; MPEs, malignant pleural effusions.

Only 9 out of 22 genes of TRMs resulted significantly up regulated in PEMC *vs* matched PBMC compared with 28 out of 37 MDMs genes (|Log2Fold Change|>2 and adjusted p<0.05) (figure 6A,B). This result suggests that TAMs in MPEs may originate from MDMs, in line with the concept that TRMs accumulate at an early phase of tumor formation and that afterwards, during tumor propagation, TME becomes dominated by MDMs.[15] Even if, for long time TAMs have been considered as tumor recruited, generally, protumoral population of differentiated monocytes that have an M2-like phenotype, it is accepted nowadays that in the TME macrophages exist on a continuum of phenotypes between classically (M1) and alternatively activated (M2).[41] Indeed, when we looked at the most up regulated genes in PEMC we identified a set of 37 genes (called MPEs Mϕ signature, see online supplemental methods and online supplemental table S2C), that do neither match with TRM nor with MDM signature (figure 6A,B) but are still related to macrophage, as shown by the analysis performed on ImmGen expression data[42] (figure 6C). The same analysis on the MDM signature gave results comparable to MPEs Mϕ signature (online supplemental figure S6A); however, with respect to the TRM signature the results clearly show that TRMs genes are specifically enriched in the alveolar macrophage populations with respect to all the other immune cell types explored (online supplemental figure S6B), thus strengthening the findings obtained on MPEs signature. The protein–protein interaction network analysis

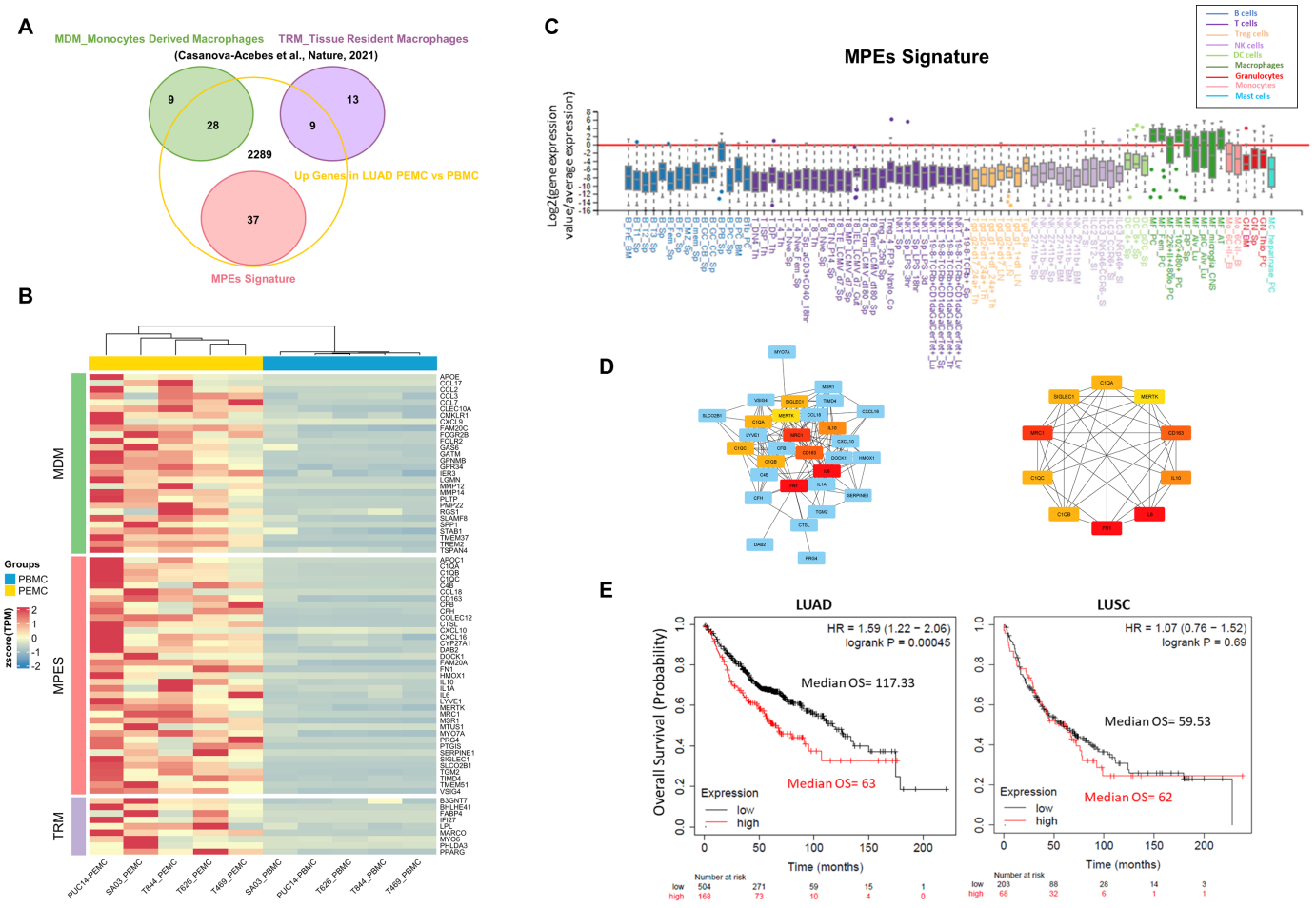

Figure 6 A novel MPE-associated gene signature correlates with poor prognosis in LUAD patients. (A) Schematic representation showing the intersection of TRM and MDM gene signatures (from Casanova-Acebes)[15] and MPEs Mϕ signature (from this study) with the up-regulated genes in LUAD PEMC versus PBMC. (B) Hierarchical clustering of TRM, MDM and MPEs Mϕ genes between LUAD PEMC versus PBMC. The heatmap reported only the genes that match with the significantly upregulated ones in PEMC (|Log2FC|>2 and adjp_val<0.05). TRM=9 out of 22; MDM=28 out of 37; MPEs Mϕ=37 out of 37. (C) RNA expression levels of the 37 genes included in the MPEs Mϕ signature across different immune cell types. Boxplots show the mean-normalized expression value of each gene in each selected cell type. The analysis was performed through My GenSet online tool. Data from http://www.immgen.org. (D) Protein-protein interaction (PPI) network built on the 37 genes included in the MPEs Mϕ signature, using STRING online database (https://string-db.org/ V.11.0). A total of 141 edges were identified (minimum required interaction score >0.4; $p<1.0 \times 10^{-16}$). Cytoscape software (V.3.8.2) was used for analysis and visualization and Cytohubba plugin app to identify the top 10 hub genes (right panel) with the highest degree of interaction. (E) Kaplan-Meier curves estimating the prognostic value of MPEs Mϕ signature in LUAD and LUSC cohorts (see online supplemental methods). A high level of MPEs Mϕ signature (red curves) was associated with poor overall survival in LUAD (p=0.00045) but not in LUSC patients (p=0.69). A p<0.05 was considered as statistically significant (log rank test). Data plotted from http://kmplot.com. LUAD, lung adenocarcinoma; LUSC, lung squamous cell carcinoma; MDM, monocytes derived macrophages; MPEs, malignant pleural effusions; PBMC, peripheral blood mononuclear cells; PEMC, pleural effusion mononuclear cells; TRM, tissue resident macrophage.

identified 37 nodes and 141 edges among the 37 genes included in the MPEs Mϕ signature (figure 6D), demonstrating that these genes are strictly interrelated. Furthermore, the CytoHubba analysis allowed to identify the top 10 nodes ranked by the degree of interactions (figure 6D, right panel). Among the identified hub genes, in which it was possible to find genes classically related to M2 phenotype (ie, CD163, MRC1, IL10), both fibronectin (FN1) and IL-6 (one of the most abundant cytokine in MPEs) showed the highest degree of interactions, resulting as potentially crucial genes.

Even if no significant differences were observed in the distribution of the MPEs Mϕ signature across different tumor stages (online supplemental figure S7), given the importance that the immune contexture may exert in the prediction of patients' outcomes,[12] we stratified 672 LUAD patients and 271 lung squamous cell carcinoma (LUSC) patients from KM Plotter database[43] according to the mean expression of the MPEs Mϕ signature . As shown by the Kaplan-Meier curves, a significant survival disadvantage was observed in patients with high expression of the MPEs Mϕ signature in LUAD but not in LUSC

(figure 6E), indicating an histotype specificity for the identified signature. Similar but less impressive results were obtained by testing the MDM signature (online supplemental figure S6C) and no significant results were obtained from the TRM signature (online supplemental figure S6D), suggesting that the newly MPEs Mϕ signature identified in this study better represents myeloid targets for the treatment of metastatic LUAD.

DISCUSSION

The implication of TIME as a key element determining resistance to immunotherapy with ICIs is now widely appreciated.[44] Furthermore the metastatic involvement of pleural and peritoneal cavities was found to be associated with worse ICIs outcome in cancer patients.[45] In this context, the past few years have witnessed a series of studies reporting a complete characterization of tumor immune landscape in NSCLC from early to advanced disease.[7 10 15 18–20] Here we performed a deep characterization of immune cells and soluble factors from MPEs and peripheral blood of LUAD patients to investigate the TIME of advanced NSCLC in a metastatic setting more easily accessible than others and, to our knowledge, still little explored.

All our observations concur to define an MPEs-specific microenvironment potentially prone to an effective immune-response, but conscripted in a wound-healing, proinflammatory and tumor-supportive mode. This is witnessed first by upregulation in PEMC, respect to the circulating PBMC counterpart, of genes related to (1) tumor promotion, spanning from angiogenesis and extracellular matrix organization (such as VEGFA, SERPINE1, FN1 and members of matrix metalloproteinase family) to cellular proliferation (such as LIF, FGF and WNT growth factors, also linked to the maintenance of tumor stem cells properties); (2) activation of chronic inflammation and immune suppression (such as IL6, IL1A, CCL3, IL10 and IDO1); (3) recruitment of TAMs, T Regs and MDSCs (such as CCL2, CCL7, CXCL1, CXCL2, CCL20); and parallel downregulation of genes (such as PRF1 and granzymes) related to the activation of effector cytotoxic cells (ie, CTL and NK cells). In accordance in silico immune deconvolution revealed a decreasing trend in the overall content of all effector cells (T and B lymphocytes and NK cells) in MPEs. On the other hand, the high proportion of monocytes, M2 polarized macrophages and activated mast cells suggests that these three immune cell types, well known to be involved in inflammatory, proangiogenic, metastatic and immune suppressive pathways,[11 46 47] could represent the major drivers in shaping an immunosuppressive MPEs microenvironment. Indeed, the presence, even if in a relatively low levels, of potent effector cytokines such as INFα2, MIP1α, INFγ and TNFβ, is a further hint of a present but thwarted immune response in the TME of MPEs. Instead, the most represented and characteristic soluble factors in MPEs are related to inflammatory processes, tumor propagation and stem like phenotype maintenance and Th2/M2 polarization. Of note SCF is also known to mediated mast cells recruitment and activation, via c-kit receptor, in tumor microenvironment.[48]

These findings are also coherent with the ability of cell free MPEs supernatant to induce in vitro M2 phenotype polarization. Our data are in line with previous findings that defined TAMs as the dominant immunosuppressive cell type in LUAD MPEs, leading to T cells disfunction via TGF-β.[21] Given the correlation between high macrophage infiltration and poor prognosis in several human cancers, including NSCLC,[12 13 49] these cells represent a promising target for anticancer therapies. Strategies, that aim at limiting macrophage recruitment or at reprogramming their phenotype toward an antitumor one, are currently under investigation.[50]

IL6 and CCL2 that we found at high concentration and with a large difference between intrapleural and systemic levels, suggesting that they are locally secreted and carry out a pivotal role in that specific TME, are inflammatory factors correlated to MPEs and monocytes/macrophages recruitment.[24] In particular, CCL2 was shown to be a major player in the recruitment of monocytes and M2 macrophage differentiation in MPEs of mesothelioma patients.[22] Furthermore, very recently it has been shown that the blockade of CCL2 expression could overcome the intrinsic PD-L1/PD-1 resistance in triple negative breast cancer.[51] These evidences support our hypothesis that monocytes of LUAD patients, the most abundant circulating immune cell type, are recruited via CCR2/CCL2 axis into MPEs where they switch toward a proinflammatory and protumoral phenotype. This concept is supported by several findings: (1) the upregulation of CCR2 receptor gene expression in LUAD PBMC with respect to HD PBMC; (2) higher concentration of CCL2 in MPEs with respect to plasma; (3) high amounts of M2 macrophages in MPEs, as shown by CIBERSORTx deconvolution, and finally (4) the ability of MPEs to induce macrophage M2 polarization in vitro. Even if these observations require further in vitro investigations, they suggest CCL2 as a potential key target for therapy in this clinical setting. Of note, antibodies that selectively target CCL2 or its receptor (CCR2) have completed phase I and II clinical trials showing promising results in advanced prostate and pancreatic cancers.[50] Likewise, clinical trials testing the activity of antibodies anti-IL6/IL6Rα are currently under investigations.[50] In this regard IL-6 resulted not only as one of the most represented cytokines in pleural effusions, but also as central gene in the identified MPEs Mϕ signature, along with FN1, highlighting a protumoral as well as a profibrotic phenotype, that could in turn promote the mobility of cancer cells in this metastatic site. Further investigations of this immune subtype may reveal novel tumor-immune interactions that are at the basis of metastatic process.

Although T cells have been the primary target of cancer immunotherapy, myeloid cells exhibit specific phenotypes and functions that could impact on cancer progression and immunotherapy response.[1] Noteworthy the 37-gene

MPEs Mϕ signature, identified in this study, resulted to be associated with poor clinical outcome specifically in LUAD patients. Hence approaches aiming to couple the specific targeting or reprogramming of immunosuppressive myeloid cells with immunotherapies directed to the reactivation of T cells could be a successful strategy to overcome drug resistance. In this regard a recent study showed how in cholangiocarcinoma the dual inhibition of TAM and G-MDSC potentiates ICI therapy, underpinning the importance of this type of combinatorial approach.[52]

Overall, our study reported for the first time a comprehensive and wide characterization of MPEs microenvironment in LUAD patients. Furthermore, given the potentiality to collect from MPEs both tumor and immune cells, it represents a patient-derived system that could be used to establish ex vivo co-culture models as a reliable in vitro testbed to evaluate the efficacy of new therapeutics.

Author affiliations
[1]Department of Experimental and Clinical Medicine, Magna Graecia University of Catanzaro, Catanzaro, Italy
[2]Department Clinical and Molecular Medicine, Sant' Andrea Hospital-Sapienza University of Rome, Rome, Italy
[3]Biostatistics, Bioinformatics and Clinical Trial Center, IRCCS Regina Elena National Cancer Institute, Rome, Italy
[4]Tumor Immunology and Immunotherapy Unit, IRCCS Regina Elena National Cancer Institute, Rome, Italy
[5]Department of Clinical and Molecular Medicine, Sant' Andrea Hospital-Sapienza University of Rome, Rome, Italy
[6]Preclinical Models and New Therapeutic Agents Unit, IRCCS Regina Elena National Cancer Institute, Rome, Italy
[7]Pathology Unit, IRCCS-Regina Elena National Cancer Institute, Rome, Italy
[8]SAFU Laboratory, IRCCS Regina Elena National Cancer Institute, Rome, Italy
[9]HPV-Unit, IRCCS Regina Elena National Cancer Institute, Rome, Italy
[10]Thoracic Surgery Unit, IRCCS Regina Elena National Cancer Institute, Rome, Italy
[11]Immunohematology and Transfusional Medicine Unit, IRCCS Regina Elena National Cancer Institute, Rome, Italy
[12]Thoracic Surgery Unit, Sapienza University of Rome, Rome, Italy
[13]Thoracic Surgery Unit, Sant' Andrea Hospital-Sapienza University of Rome, Rome, Italy
[14]Department of Medical Surgical Sciences and Translational Medicine, Sapienza University of Rome, Rome, Italy
[15]Takis Srl, Roma, Italy
[16]Scientific Directorate, IRCSS Regina Elena National Cancer Institute, Rome, Italy

Acknowledgements This study was supported by Italian Association for Cancer Research (AIRC), Italian Ministry of Health, Lazio Innova. SB was recipient of a PhD fellowship funding from the Ministry of Education, University and Research (MIUR), Italy, PON-FSE-FESR-Research and Innovation 2014-2020 for Doctoral studies with industrial characterization 2017. We thank all patients who donated samples for this research.

Contributors Conceptualization: GC, SB, RM and MP. Data curation, formal analysis and visualization: ES, LD'A, SB and MP. Methodology and investigation: SB, FA, CDV, VS, AE, SDM, FDN and FP. Resources: GA, FF, MLF, MB, FV, MD'A, AR, AD'A and EAR. Writing - original draft: SB. Writing- review AND editing: GC, RM, MP, LF, MF, LA and CN. Supervision: GC and RM. Project administration and funding acquisition: RM and GC. GC and RM accepted full responsibility for the study, had access to the data and controlled the decision to submit for publication. All authors read and approved the final version of the manuscript.

Funding This work was supported by the Italian Association for Cancer Research (AIRC) grants IG19865 and IG24451, respectively, to GC and RM, and by the Ministry of Education, University and Research (MIUR), grant PRIN 2017 (Prot. 2017HWTP2K) to RM. RM is also supported by Lazio Innova grants 2018 n.85-2017-13750 and 2020 n.A0375-2020-36657.This work was supported in part by Ricerca Corrente funds 2022 from Italian Ministry of Health.

Competing interests All the authors with the exception of LA have nothing to disclose. LA is an employee of Takis srl.

Patient consent for publication Not applicable.

Ethics approval This study involves human participants and was approved by Ethics Committees: IFO Institutional Research Ethics Committee(ID: Prot. Number 1032/17)Sapienza University Ethics Committee(ID: Rif. CE 6098_2020, Prot. Number 210 SA_2020ID: Rif. CE 6546, Prot. Number 0946/2021).

Provenance and peer review Not commissioned; externally peer reviewed.

Data availability statement Data are available upon reasonable request All processed data (including RNA-seq expression levels) presented in this study and all the visualizations and analysis scripts (R V.4.1.0) are available in the repository https://gitlab.com/bioinfo-ire-release/bruschini_pallocca_etal. Raw data are available upon reasonable request.

ORCID iD
Gennaro Ciliberto http://orcid.org/0000-0003-2851-8605

REFERENCES

1 Zhang Y, Zhang Z. The history and advances in cancer immunotherapy: understanding the characteristics of tumor-infiltrating immune cells and their therapeutic implications. *Cell Mol Immunol* 2020;17:807–21.
2 Doroshow DB, Sanmamed MF, Hastings K, *et al*. Immunotherapy in non-small cell lung cancer: facts and hopes. *Clin Cancer Res* 2019;25:4592–602.
3 Langer CJ, Gadgeel SM, Borghaei H, *et al*. Carboplatin and pemetrexed with or without pembrolizumab for advanced, non-squamous non-small-cell lung cancer: a randomised, phase 2 cohort of the open-label KEYNOTE-021 study. *Lancet Oncol* 2016;17:1497–508.
4 Faivre-Finn C, Vicente D, Kurata T, *et al*. Four-Year survival with Durvalumab after chemoradiotherapy in stage III NSCLC-an update from the Pacific trial. *J Thorac Oncol* 2021;16:860–7.
5 Sharma P, Hu-Lieskovan S, Wargo JA, *et al*. Primary, adaptive, and acquired resistance to cancer immunotherapy. *Cell* 2017;168:707–23.
6 Anderson NM, Simon MC. The tumor microenvironment. *Curr Biol* 2020;30:R921–5.
7 Guo X, Zhang Y, Zheng L, *et al*. Global characterization of T cells in non-small-cell lung cancer by single-cell sequencing. *Nat Med* 2018;24:978–85.
8 Patil NS, Nabet BY, Müller S, *et al*. Intratumoral plasma cells predict outcomes to PD-L1 blockade in non-small cell lung cancer. *Cancer Cell* 2022;40:289–300.
9 Datta M, Coussens LM, Nishikawa H, *et al*. Reprogramming the tumor microenvironment to improve immunotherapy: emerging strategies and combination therapies. *Am Soc Clin Oncol Educ Book* 2019;39:165–74.
10 Lavin Y, Kobayashi S, Leader A, *et al*. Innate immune landscape in early lung adenocarcinoma by paired single-cell analyses. *Cell* 2017;169:750–65.
11 Cassetta L, Fragkogianni S, Sims AH, *et al*. Human tumor-associated macrophage and monocyte transcriptional landscapes reveal cancer-specific reprogramming, biomarkers, and therapeutic targets. *Cancer Cell* 2019;35:588–602.

12 Bruni D, Angell HK, Galon J. The immune contexture and immunoscore in cancer prognosis and therapeutic efficacy. *Nat Rev Cancer* 2020;20:662–80.
13 Cassetta L, Pollard JW. Targeting macrophages: therapeutic approaches in cancer. *Nat Rev Drug Discov* 2018;17:887–904.
14 Duan Z, Luo Y. Targeting macrophages in cancer immunotherapy. *Sig Transduct Target Ther* 2021;6:1–21.
15 Casanova-Acebes M, Dalla E, Leader AM, *et al*. Tissue-resident macrophages provide a pro-tumorigenic niche to early NSCLC cells. *Nature* 2021;595:578–84.
16 Penz E, Watt KN, Hergott CA, *et al*. Management of malignant pleural effusion: challenges and solutions. *Cancer Manag Res* 2017;9:229–41.
17 Psallidas I, Kalomenidis I, Porcel JM, *et al*. Malignant pleural effusion: from bench to bedside. *Eur Respir Rev* 2016;25:189–98.
18 Lambrechts D, Wauters E, Boeckx B, *et al*. Phenotype molding of stromal cells in the lung tumor microenvironment. *Nat Med* 2018;24:1277–89.
19 Kim N, Kim HK, Lee K, *et al*. Single-cell RNA sequencing demonstrates the molecular and cellular reprogramming of metastatic lung adenocarcinoma. *Nat Commun* 2020;11:1–15.
20 Wu F, Fan J, He Y, *et al*. Single-cell profiling of tumor heterogeneity and the microenvironment in advanced non-small cell lung cancer. *Nat Commun* 2021;12:1–11.
21 Li L, Yang L, Wang L, *et al*. Impaired T cell function in malignant pleural effusion is caused by TGF-β derived predominantly from macrophages. *Int J Cancer* 2016;139:2261–9.
22 Chéné A-L, d'Almeida S, Blondy T, *et al*. Pleural effusions from patients with mesothelioma induce recruitment of monocytes and their differentiation into M2 macrophages. *J Thorac Oncol* 2016;11:1765–73.
23 Nieto JC, Zamora C, Porcel JM, *et al*. Migrated T lymphocytes into malignant pleural effusions: an indicator of good prognosis in lung adenocarcinoma patients. *Sci Rep* 2019;9:1–11.
24 Donnenberg AD, Luketich JD, Dhupar R, *et al*. Treatment of malignant pleural effusions: the case for localized immunotherapy. *Journal for ImmunoTherapy of Cancer* 2019;7:5–9.
25 Mancini R, Giarnieri E, De Vitis C, *et al*. Spheres derived from lung adenocarcinoma pleural effusions: molecular characterization and tumor engraftment. *PLoS One* 2011;6:e21320.
26 Noto A, De Vitis C, Pisanu ME, *et al*. Stearoyl-CoA-desaturase 1 regulates lung cancer stemness via stabilization and nuclear localization of YAP/TAZ. *Oncogene* 2017;36:4573–84.
27 Bruschini S, di Martino S, Pisanu ME, *et al*. Cytomatrix for a reliable and simple characterization of lung cancer stem cells from malignant pleural effusions. *J Cell Physiol* 2020;235:1877–87.
28 De Vitis C, Corleone G, Salvati V. B4GALT1 is a new candidate to maintain the stemness of lung cancer stem cells. *J Clin Med* 1928;2019:8.
29 Di Martile M, Farini V, Consonni FM, *et al*. Melanoma-specific bcl-2 promotes a protumoral M2-like phenotype by tumor-associated macrophages. *J Immunother Cancer* 2020;8:e000489.
30 Sperandio E, Grassucci I, D'Ambrosio L. Automated, reproducible investigation of gene set differential enrichment via the AUTO-go framework. *bioRxiv* 2022;2022:482003.
31 Newman AM, Steen CB, Liu CL, *et al*. Determining cell type abundance and expression from bulk tissues with digital cytometry. *Nat Biotechnol* 2019;37:773–82.
32 Kleiveland C, Kleiveland C. Peripheral blood mononuclear cells. *Impact Food Bioact Heal Vitr Ex Vivo Model* 2015:161–7.
33 Geissmann F, Jung S, Littman DR. Blood monocytes consist of two principal subsets with distinct migratory properties. *Immunity* 2003;19:71–82.
34 Qian B-Z, Li J, Zhang H, *et al*. CCL2 recruits inflammatory monocytes to facilitate breast-tumour metastasis. *Nature* 2011;475:222–5.
35 Kaminska J, Kowalska M, Kotowicz B, *et al*. Pretreatment serum levels of cytokines and cytokine receptors in patients with non-small cell lung cancer, and correlations with clinicopathological features and prognosis. *Oncology* 2006;70:115–25.
36 Levina V, Marrangoni AM, DeMarco R, *et al*. Drug-selected human lung cancer stem cells: cytokine network, tumorigenic and metastatic properties. *PLoS One* 2008;3:e3077.
37 Levina V, Marrangoni A, Wang T, *et al*. Elimination of human lung cancer stem cells through targeting of the stem cell factor-c-kit autocrine signaling loop. *Cancer Res* 2010;70:338–46.
38 Kaplanski G, Marin V, Montero-Julian F. IL-6: a regulator of the transition from neutrophil to monocyte recruitment during inflammation. *Trends Immunol* 2003;24:25–9.
39 Mills CD, Kincaid K, Alt JM, *et al*. M-1/M-2 macrophages and the Th1/Th2 paradigm. *J Immunol* 2000;164:6166–73.
40 Spranger S, Dai D, Horton B, *et al*. Tumor-residing Batf3 dendritic cells are required for effector T cell trafficking and adoptive T cell therapy. *Cancer Cell* 2017;31:711–23.
41 Wagner J, Rapsomaniki MA, Chevrier S, *et al*. A single-cell atlas of the tumor and immune ecosystem of human breast cancer. *Cell* 2019;177:1330–45.
42 Aguilar SV, Aguilar O, Allan R, *et al*. ImmGen at 15. *Nat Immunol* 2020;21:700–3.
43 Győrffy B, Surowiak P, Budczies J, *et al*. Online survival analysis software to assess the prognostic value of biomarkers using transcriptomic data in non-small-cell lung cancer. *PLoS One* 2013;8:e82241.
44 Binnewies M, Roberts EW, Kersten K, *et al*. Understanding the tumor immune microenvironment (TIME) for effective therapy. *Nat Med* 2018;24:541–50.
45 Chow A, Schad S, Green MD, *et al*. Tim-4+ cavity-resident macrophages impair anti-tumor CD8+ T cell immunity. *Cancer Cell* 2021;39:973–88.
46 Marichal T, Tsai M, Galli SJ. Mast cells: potential positive and negative roles in tumor biology. *Cancer Immunol Res* 2013;1:269–79.
47 Chittezhath M, Dhillon MK, Lim JY, *et al*. Molecular profiling reveals a tumor-promoting phenotype of monocytes and macrophages in human cancer progression. *Immunity* 2014;41:815–29.
48 Huang B, Lei Z, Zhang G-M, *et al*. SCF-mediated mast cell infiltration and activation exacerbate the inflammation and immunosuppression in tumor microenvironment. *Blood* 2008;112:1269–79.
49 Mei J, Xiao Z, Guo C, *et al*. Prognostic impact of tumor-associated macrophage infiltration in non-small cell lung cancer: a systemic review and meta-analysis. *Oncotarget* 2016;7:34217–28.
50 Bejarano L, Jordão MJC, Joyce JA. Therapeutic targeting of the tumor microenvironment. *Cancer Discov* 2021;11:933–59.
51 Choi J, Lee HJ, Yoon S, *et al*. Blockade of CCL2 expression overcomes intrinsic PD-1/PD-L1 inhibitor-resistance in transglutaminase 2-induced PD-L1 positive triple negative breast cancer. *Am J Cancer Res* 2020;10:2878–94.
52 Loeuillard E, Yang J, Buckarma E, *et al*. Targeting tumor-associated macrophages and granulocytic myeloid-derived suppressor cells augments PD-1 blockade in cholangiocarcinoma. *J Clin Invest* 2020;130:5380–96.

Supplementary Methods

PEMC and PBMC isolation from LUAD patients and HD

MPEs were obtained by thoracentesis and collected aseptically in non heparinized bottles/tubes. After a centrifugation step (1,200 rpm for 5min at 4°C) supernatants were harvested and stored at -80°C. The cell fraction was collected, washed twice with phosphate-buffered saline (PBS; Sigma, St. Louis, MO) by centrifugation (1,200 rpm for 5min at 4°C), layered on OncoQuick gradient separation medium (Greiner Bio-One) and centrifuged (1,600 g, no brake, for 20 min at 4°C) to partially purify tumour cells, that are enriched at the interphase layer of the gradient, from erythrocytes and leucocytes that migrate into the lower phase through the bottom of the tube. To further separate erythrocytes from pleural effusion mononuclear cells (PEMC), cells derived from the lower phase were resuspended in PBS and further stratified on Lympholyte-H density gradient separation medium (Cedarlane, Ontario, CA, USA). After a centrifugation step (1,800 rpm, no brake, for 20 min at room temperature) PEMC fraction (ring) were collected, washed twice with PBS and frozen in 10% v/v DMSO, 90% v/v fetal bovine serum (FBS) solution (Sigma-Aldrich, St. Louis, MO) for subsequent RNA extraction.

Peripheral blood was collected from LUAD patients and healthy donors (HD) in anti-coagulant supplemented blood tubes and centrifuged (1,800 rpm for 10 min at 4°C) to separate cells from plasma. Plasma was then collected and stored at -80°C and cells were stratified on Lympholyte-H density gradient separation medium to isolate mononuclear cells (PBMC).

Bulk RNA Sequencing (RNA-Seq), data processing, DEGs identification and functional enrichment analysis

RNA libraries for sequencing were generated using the TruSeq RNA Exome kit (Illumina, San Diego, CA, USA), optimized for low input and low-quality RNA. The procedure consists of a general whole transcriptome strand specific library preparation followed by a specific exon targeting enrichment. The quality of the resulting libraries was assessed via Bioanalyzer (High Sensitivity DNA Kit). The intermediate library, before exon enrichment, was quantified by Qubit, the final library by qPCR. Samples were sequenced in paired-end mode, sequencing 76 bp from each side, with NextSeq 500 System (Illumina).

RNA-seq raw data were processed thanks to the nf-core/rnaseq pipeline (v 2.4)[1], which carries out the primary analysis of the mapping onto the reference genome (GRCh37) providing Quality Control metrics of the analysed samples, obtaining both the raw counts (FeatureCounts) and the TPM (Transcript Per Million) normalized pseudo counts. The DEseq2 Bioconductor package[2] was used to test for the differentially expressed genes (DEGs) between the groups using the negative binomial

distribution and Wald's test. For DEG identification, genes with an adjusted p-value < 0.05 were considered as statistically significant and an additional filter cut-off criterion of | log2FC|> 2 was applied to select the signature with the strongest induction among conditions. The biological function of DEGs was identified by Gene Ontology (GO) analysis using the R package "enrichR"[3]. GO visualizations were produced via the auto-GO/ARGO framework. Fisher's exact test was employed, and the occurrence of false positives was corrected by Benjamini-Hochberg (B-H) multiple test correction method. For the enrichment analysis, an adjusted p-value < 0.05 was set as the cut-off criterion.

MPEs Mφ signature: ImmGen interrogation and network analysis

As a starting point for the selection of the MPEs Mφ signature we used the upregulated genes in LUAD PEMC compared to matched PBMC (n=2363 Log2FC >2 and adjusted p-value < 0.05), exploiting the fact that the macrophagic component is present only at the tumour site (i.e. MPEs) and not in the circulation. Subsequently additional filter cut-off criteria, log2FC ≥ 3 and mean_PEMC_≥ 10 (where mean stands for mean of the normalized values with the variance stabilizing transformation, vsd () function, of DeSeq), were applied to select the genes with the strongest induction in PEMC. After filtering, 194 genes were selected. Finally in order to identify the most relevant genes related to macrophage phenotype we used the public ImmGen (Immunological Genome Project)[4,5] resources available online (http://www.immgen.org), obtaining a 37 gene list (MPEs Mφ signature, Table S2). My Gene Set browser was used to examine the expression pattern of the identified genes across different immune cell types, exploiting the ImmGen expression data. In detail, the ImmGen ULI RNA-seq dataset GSE127267, that encompasses primary RNAseq data from carefully sorted immunocyte populations, sequenced using ImmGen's SOP for 'ultra-low-input' population RNAseq (typically 500 to 1,000 cells) performed by Smartseq2, was used to test MPEs Mφ signature as well as TMR and MDM signatures[6] and to generate the reported graphs (Figure 5 and Supplementary Figure S6).

Gene expression data of 505 LUAD patients were downloaded from Xena Browser[7] as RSEM_TPM log2 (tpm+0.001) and transformed applying the (2^tpm)-0.001 formula to then calculate the geometric mean of the 37 genes expression (MPEs Mφ signature) across all patients, divided into different stage disease. Stage I (N=274), Stage II (N=122), Stage III (N=83), Stage IV (N=26).

The protein-protein interaction (PPI) networks for the 37 genes included in the MPEs Mφ signature was constructed using the Search Tool for the Retrieval of Interacting Genes (STRING) online database[8] (http://string-db.org; version11.0). An interaction score > 0.4 was regarded as statistically significant. The molecular interaction network was visualized using Cytoscape[9]

software (v 3.8.2) and the Cytohubba plugin app[10] within Cytoscape was used to calculate degree of interaction between these 37 genes. The top 10 genes were defined as hub genes.

Survival analyses

Survival analyses were performed using the KM-plotter database (http://kmplot.com)[11]. Kaplan–Meier curves stratify 672 LUAD and 271 LUSC patients by high and low MPEs Mφ signature expression. The upper quartile value was used as cut-off criterion. $p < 0.05$ was considered as statistically significant (log rank test).

The analyses were performed on expression data from tissue biopsies of 672 independent patient samples from seven LUAD cohorts: GSE19188, GSE29013, GSE30219, GSE31210, GSE3141, GSE37745, GSE50081; and on 271 independent patient samples from six LUSC cohorts: GSE19188, GSE29013, GSE30219, GSE3141, GSE37745, GSE50081. The main clinical characteristics of those patients are reported in the table below:

Dataset	Cancer Type	Sex	Median Age	Disease Stage
GSE19188	LUAD (N=40)	M (N=25);F(N=15)	N/A	I-II
	LUSC (N=24)	M (N=22); F(N=2)	N/A	I-II
GSE29013	LUAD (N=30)	M (N=20);F(N=10)	66	I(N=16)-II(N=6)-III(N=8)
	LUSC (N=25)	M (N=18); F(N=7)	65	I(N=8)-II(N=8)-III(N=9)
GSE30219	LUAD (N=85)	M (N=67);F(N=18)	60	N/A
	LUSC (N=61)	M (N=57); F(N=4)	63	N/A
GSE3141	LUAD (N=58)	N/A	N/A	N/A
	LUSC (N=53)	N/A	N/A	N/A
GSE37745	LUAD (N=106)	M (N=46);F(N=60)	64	I(N=70)-II(N=19)-III(N=13)-IV(=4)
	LUSC (N=66)	M (N=46);F(N=20)	67	I(N=40)-II(N=15)-III(N=11)
GSE50081	LUAD (N=127)	M (N=65);F(N=62)	70	I(N=92)-II(N=35)
	LUSC (N=42)	M (N=24);F(N=18)	70	I(N=26)-II(N=16)
GSE31210	LUAD (N=226)	M (N=105); F(N=121)	61	I(N=168)-II(N=58)

THP1-Monocytes differentiation and MPEs stimulation

Human THP-1 monocytes were maintained in culture medium RPMI-1640 (Sigma-Aldrich, St. Louis, MO) supplemented with 10% of inactivated FBS and incubated at 37°C in a 5% v/v CO2 atmosphere. For monocyte-macrophage differentiation, cells were seeded at a density of $1x10^5$ cells/ml in 6-well plates and macrophage differentiation was initiated by exposing the cells to 100ng/ml phorbol-12-myristate-13-acetate (PMA) (Sigma-Aldrich) in 10% FBS culture medium for 24 hours. Subsequently, THP-1 derived macrophages were cultured for 48 hours with serum free medium (M0 macrophages) or medium supplemented with 10% of cell-free pleural fluids from LUAD patients. M1/M2 polarization was then assessed by qRT-PCR. Experiments were performed

independently at least three times and the data were expressed as average ± SE of the mean (SEM). Differences between groups were analysed with a two-tailed Student's t-test and were considered statistically significant for p-value <0.05

Cytokine Array

Levels of 48 different cytokines, including chemokines, interleukins and growth factors, were evaluated at the same time in cell-free pleural fluids and matched plasma of 15 LUAD patients and in plasma of 4 HDs, using Pro Human Cytokine Screening 48-Plex Assays panel (Bio-Rad, Hercules, CA, USA), according to the manufacturer's instructions.

Immediately prior to the analysis, the frozen samples were thawed and clarified by centrifugation (15 min at 1,000 x g) in a cold room environment (4°C). Pleural fluid samples were also filtered through a 0.2 µm filter prior to the analysis. Cytokines were quantified on the Luminex platform using the Bio-Plex MagPix instrument (Bio-Rad, Hercules, CA, USA) and the Bio-Plex Manager MP software was used for data acquisition and analysis. All the samples were run in duplicate and ten-point standard curve was run for each cytokine. Determinations that were designated "Out of Range Below" (i.e. below the limit of quantification) by the analytical software were arbitrarily filled with a zero value. Cytokines fold change, calculated as the ratio between cytokine levels in pleural fluid samples with respect to those in matched plasma samples of LUAD patients, were considered statistically significant if p-value < 0.05 (two-tailed Student's t-test). For the complete list of 48 analysed cytokines see Supplementary Table S5.

Wound healing assays

Wound healing assays were performed on two MPEs-derived primary cell lines (i.e BBIRE-T248 and PUC36) isolated and characterized as previously reported[12]. Primary cells were cultured in RPMI-1640 (Sigma-Aldrich, St. Louis, MO) supplemented with 10% FBS and incubated at 37°C in a 5% v/v CO2 atmosphere. For wound healing assay 9 x 10^4 cells were plated into a 2 well culture-insert (Ibidi GmbH, Martinsried, Germany). When cells reached complete confluence, the culture-insert was removed, cells were washed with PBS, and cultured for 24 hours with serum free medium (CTRL) or medium supplemented with 10% of matched cell-free pleural fluids. Images were captured immediately after insert removal (T0) and after 24 hours of treatment (T24), with an Axiocam 208 color (Zeiss, Oberkochen, Germany), coupled with a ZEISS Primovert Photo optical microscope (Zeiss, Oberkochen, Germany). The cell-free space (open residual area) was measured by using the ImageJ software (NIH, Rockville, USA). Experiments were performed independently at least three times and the data were expressed as average ± SE of the mean (SEM). Differences between groups

were analysed with paired Student's t-test and were considered statistically significant for p-value <0.05.

List of the Online Tools Used

http://string-db.org

http://www.immgen.org

http://kmplot.com

https://cibersortx.stanford.edu

Supplementary References

1. Ewels PA, Peltzer A, Fillinger S, et al. The nf-core framework for community-curated bioinformatics pipelines. Nat. Biotechnol. 2020; p. 276–8.

2. Love MI, Huber W, Anders S. Moderated estimation of fold change and dispersion for RNA-seq data with DESeq2. Genome Biol. 2014;15:550.

3. Kuleshov M V., Jones MR, Rouillard AD, et al. Enrichr: a comprehensive gene set enrichment analysis web server 2016 update. Nucleic Acids Res. 2016;44:W90–7.

4. Aguilar SV, Aguilar O, Allan R, et al. ImmGen at 15. Nat. Immunol. 2020; p. 700–3.

5. Heng TSP, Painter MW, Elpek K, et al. The immunological genome project: Networks of gene expression in immune cells. Nat. Immunol. 2008; p. 1091–4.

6. Casanova-Acebes M, Dalla E, Leader AM, et al. Tissue-resident macrophages provide a pro-tumorigenic niche to early NSCLC cells. Nature. 2021;595:578–84.

7. Goldman MJ, Craft B, Hastie M, Repečka K, McDade F, Kamath A, et al. Visualizing and interpreting cancer genomics data via the Xena platform. Nat. Biotechnol. 2020. p. 675–8.

8. Szklarczyk D, Gable AL, Lyon D, et al. STRING v11: protein-protein association networks with increased coverage, supporting functional discovery in genome-wide experimental datasets. Nucleic Acids Res. 2019;47:D607–13.

9. Shannon P, Markiel A, Ozier O, et al. Cytoscape: a software environment for integrated models of biomolecular interaction networks. Genome Res. 2003;13:2498–504.

10. Chin CH, Chen SH, Wu HH, Ho CW, Ko MT, Lin CY. cytoHubba: identifying hub objects and sub-networks from complex interactome. BioMed Central. 2014;8:S11.

11. Győrffy B, Surowiak P, Budczies J, Lánczky A. Online Survival Analysis Software to Assess the Prognostic Value of Biomarkers Using Transcriptomic Data in Non-Small-Cell Lung Cancer. PLoS One. 2013;8:e82241.

12. Bruschini S, di Martino S, Pisanu ME, Fattore L, De Vitis C, Laquintana V, et al. CytoMatrix for a reliable and simple characterization of lung cancer stem cells from malignant pleural effusions. J Cell Physiol. 2020;235:1877–87.

Supplementary Figure S1. (**A**) Hierarchical clustering of all differentially expressed genes (DEGs) between LUAD PBMC (n=5) and HD PBMC (n=4). Expression values are Z score transformed. Samples were clustered using complete linkage and Euclidean distance. (**B**) Volcano plot showing upregulated (red dots) and downregulated genes (green dots) resulted from the differential expression analysis performed on LUAD PBMC *vs* HD PBMC. Only genes with |Log2FC| >2 and adjp_val < 0.05 were considered significantly deregulated. Some of the most relevant genes are reported. (**C**) Gene Ontology (GO) analysis of downregulated genes (upper panel) and upregulated genes (lower panel) in LUAD PBMC *vs* HD PBMC. Terms over red dashed line are considered statistically significant (adjp_val < 0.05). (**D**) qRT-PCR validation showing mRNA levels in LUAD PBMC (blue) compared to HD PBMC (red) of some selected proinflammatory cytokines and chemokines genes (GAPDH was used as housekeeping gene). The box plot represents minimum and maximum values (whiskers), median values (center lines), mean values (center aterisk) and 25th and 75th percentiles (box edges), with all data points plotted. Each dot represents one patient (healthy: n= 8; patients: n=14). *p < 0.05, ***p < 0.001 and ****p < 0.0001 (Wilcoxon Signed Rank Sum Test). LUAD, lung adenocarcinoma; HD, healthy donors; PBMC, peripheral blood mononuclear cells; FC, fold change; adjp_val; adjusted p_value.

Supplementary Figure S2. (A) Bar plots of selected deregulated genes, from RNA-Seq, in LUAD PEMC *vs* PBMC (|Log2FC| >2 and adjp_val < 0.05). The selected genes were grouped into three main clusters: growth factors and metastatic angiogenic promoters (left panel), proinflammatory chemokines (middle panel) and cytokines/enzymes related to the regulation of the immune response (right panel). (**B**) qRT-PCR analyses confirming the upregulation of proinflammatory cytokines and chemokines genes in LUAD PEMC (yellow) *vs* matched PBMC (blue). GAPDH was used as housekeeping gene. The box plot represents minimum and maximum values (whiskers), median values (center lines), mean values (center aterisk) and 25th and 75th percentiles (box edges), with all data points plotted. Each dot represents one patient (n=14). *p < 0.05, **p < 0.01 and ***p < 0.001 (Wilcoxon Signed Rank Sum Test). LUAD, lung adenocarcinoma; PEMC, pleural effusion mononuclear cells; PBMC, peripheral blood mononuclear cells; FC, fold change; adjp_val; adjusted p_value.

Supplementary Figure S3. Dot plots showing the differential deconvolution analysis performed on lymphoid and myeloid subsets between the three sample groups. Each dot represents one patient. Mean values of CIBERSORTx absolute scores and standard deviations for each cell subset were calculated for each patient group and compared using paired (LUAD PEMC vs PBMC) or unpaired (LUAD PBMC vs HD) two-tailed Student's t-test. *$p < 0.05$; **$p < 0.01$. LUAD, lung adenocarcinoma; HD, healthy donors; PBMC, peripheral blood mononuclear cells; PEMC, pleural effusion mononuclear cells.

Supplementary Figure S4. LUAD and HD plasma are characterized by similar cytokine pattern. Scatter plots showing the mean values ± SEM of cytokines concentration (pg/ml), evaluated in plasma of 15 LUAD patients and 4 HD. LUAD, lung adenocarcinoma; HD, healthy donors.

Supplementary Figure S5. Representative images of wound healing assay of two MPE-derived primary cell lines, BBIRE-T248 (A) and PUC 36 (B), stimulated with 10% of their matched cell free MPEs and respective non-treated cells (CTRL), immediately after insert removal (T0) and after 24 hours (T24) of treatment. Magnification: 4X. (C) Percentage of open residual wound area after 24 hours (T24) respect to T0 in BBIRE-T248 and PUC 36 (D) treated cells (MPEs) and in the respective non-treated cells. The mean ± SEM of three independent experiments is reported. *$p < 0.05$; and ****$p < 0.0001$ (paired Student's t-test).

Supplementary Figure S6. RNA expression levels of MDM (**A**) and TRM (**B**) signatures are tested across different immune cell types. Boxplots show the mean-normalized expression value of each gene in each selected cell type. The analysis was performed through My GenSet online tool. Data from http://www.immgen.org. (**C**) Kaplan Meier analysis of overall survival comparing LUAD patients with high (red curves) and low (black curves) expression of MDM and TRM (**D**) signatures. $p < 0.05$ was considered as statistically significant (log rank test). Data Plotted from http://kmplot.com. LUAD, lung adenocarcinoma; TRM, tissue resident macrophages; MDM, monocytes derived macrophages.

Supplementary Figure S7. Box plots representing the mean expression values of the MPEs Mφ signature across different LUAD stages. Stage I (patients: n=274), Stage II (patients: n=122), Stage III (patients: n=83), Stage IV (patients: n=26).

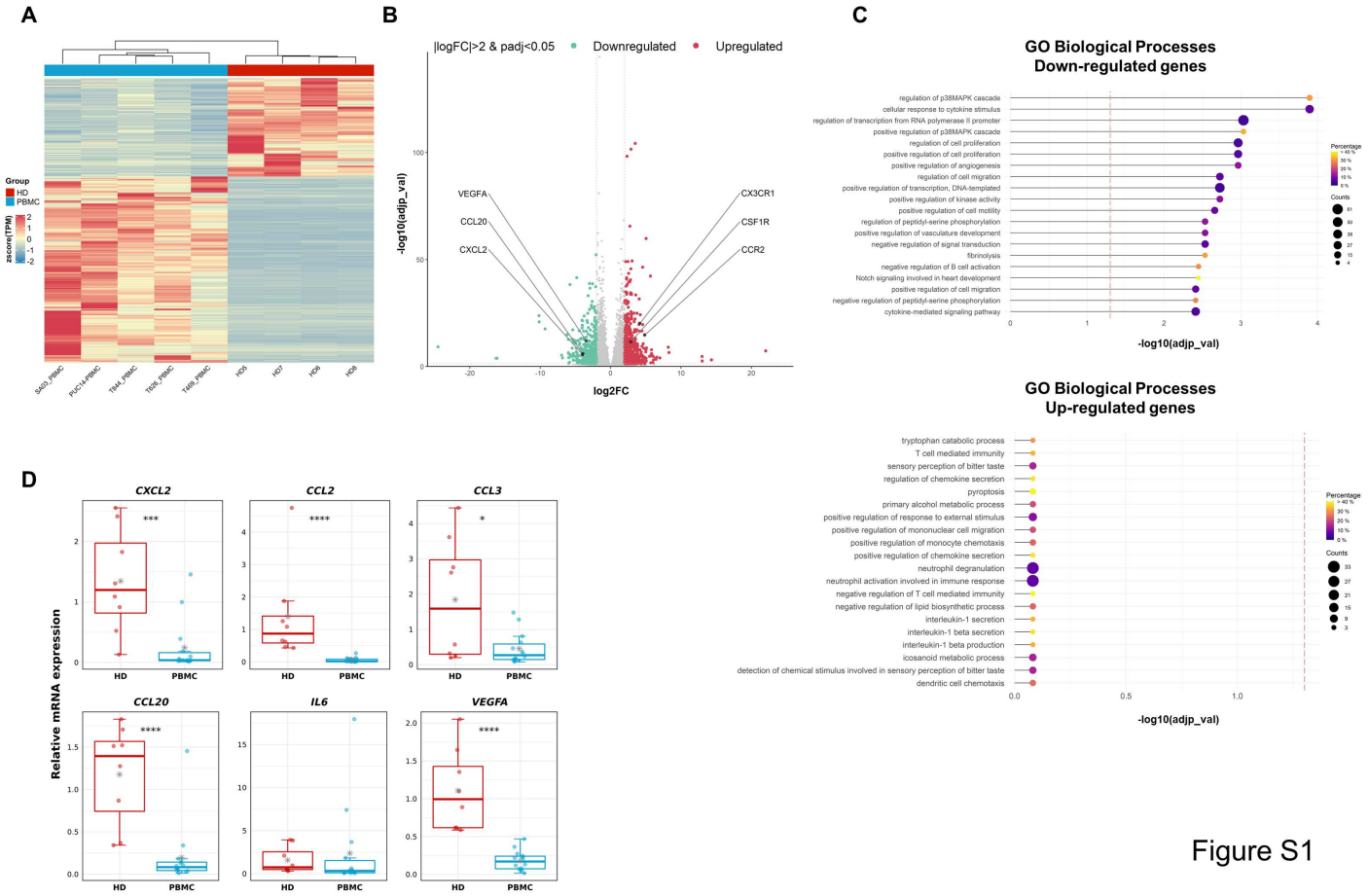
A
B
C
Group
HD
PBMC
zscore(TPM)
||logFC|>2 & padj<0.05
Downregulated
Upregulated
-log10(adjp_val)
log2FC
VEGFA
CCL20
CXCL2
CX3CR1
CSF1R
CCR2
GO Biological Processes
Down-regulated genes
regulation of p38MAPK cascade
cellular response to cytokine stimulus
regulation of transcription from RNA polymerase II promoter
positive regulation of p38MAPK cascade
regulation of cell proliferation
positive regulation of cell proliferation
positive regulation of angiogenesis
regulation of cell migration
positive regulation of transcription, DNA-templated
positive regulation of kinase activity
positive regulation of cell motility
regulation of peptidyl-serine phosphorylation
positive regulation of vasculature development
negative regulation of signal transduction
fibrinolysis
negative regulation of B cell activation
Notch signaling involved in heart development
positive regulation of cell migration
negative regulation of peptidyl-serine phosphorylation
cytokine-mediated signaling pathway
-log10(adjp_val)
Percentage
Counts
GO Biological Processes
Up-regulated genes
tryptophan catabolic process
T cell mediated immunity
sensory perception of bitter taste
regulation of chemokine secretion
pyroptosis
primary alcohol metabolic process
positive regulation of response to external stimulus
positive regulation of mononuclear cell migration
positive regulation of monocyte chemotaxis
positive regulation of chemokine secretion
neutrophil degranulation
neutrophil activation involved in immune response
negative regulation of T cell mediated immunity
negative regulation of lipid biosynthetic process
interleukin-1 secretion
interleukin-1 beta secretion
interleukin-1 beta production
icosanoid metabolic process
detection of chemical stimulus involved in sensory perception of bitter taste
dendritic cell chemotaxis
-log10(adjp_val)
Percentage
Counts
D
CXCL2
CCL2
CCL3
CCL20
IL6
VEGFA
Relative mRNA expression
HD
PBMC

Figure S1

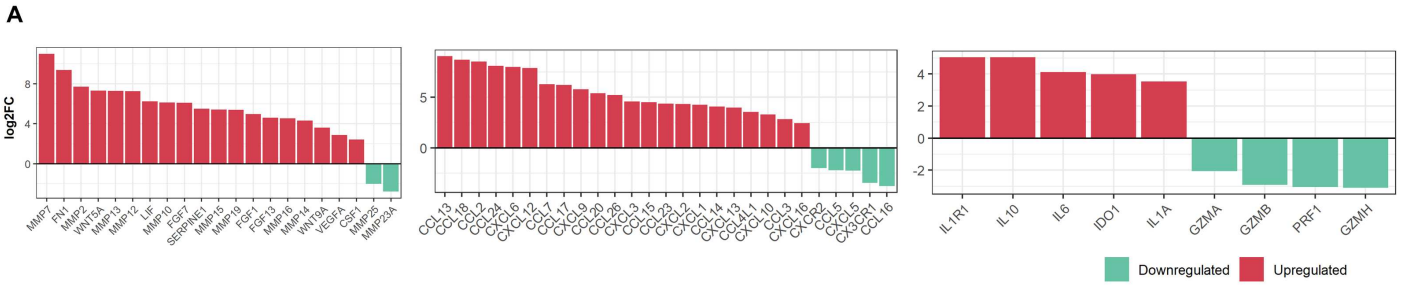
A
log2FC
MMP7 FN1 MMP2 WNT5A MMP13 MMP12 LIF MMP10 FGF7 SERPINE1 MMP15 MMP19 FGF1 FGF13 MMP16 MMP14 WNT9A VEGFA CSF1 MMP25 MMP23A
CCL13 CCL18 CCL2 CCL24 CXCL6 CXCL12 CCL7 CCL17 CXCL9 CCL26 CXCL3 CCL15 CCL23 CXCL2 CXCL1 CCL14 CXCL13 CCL4L1 CXCL10 CCL3 CXCL16 CXCR2 CCL5 CXCL5 CX3CR1 CCL16
IL1RI IL10 IL6 IDO1 IL1A GZMA GZMB PRF1 GZMH
Downregulated
Upregulated

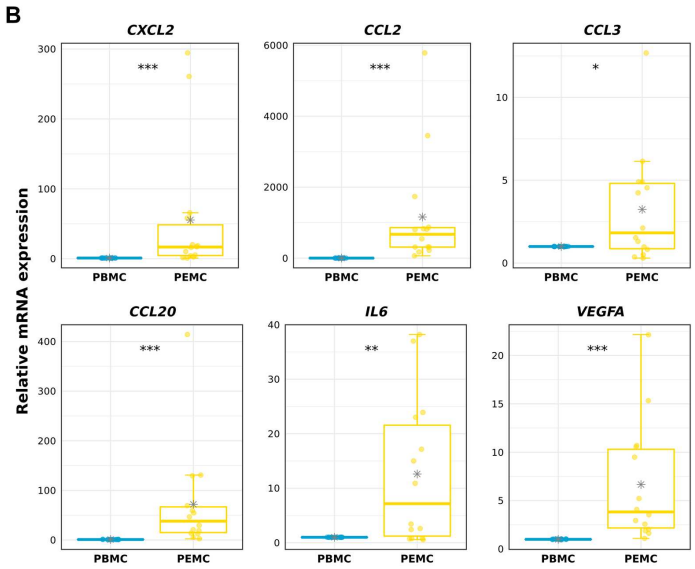
B
CXCL2
CCL2
CCL3
CCL20
IL6
VEGFA
Relative mRNA expression
PBMC
PEMC

Figure S2

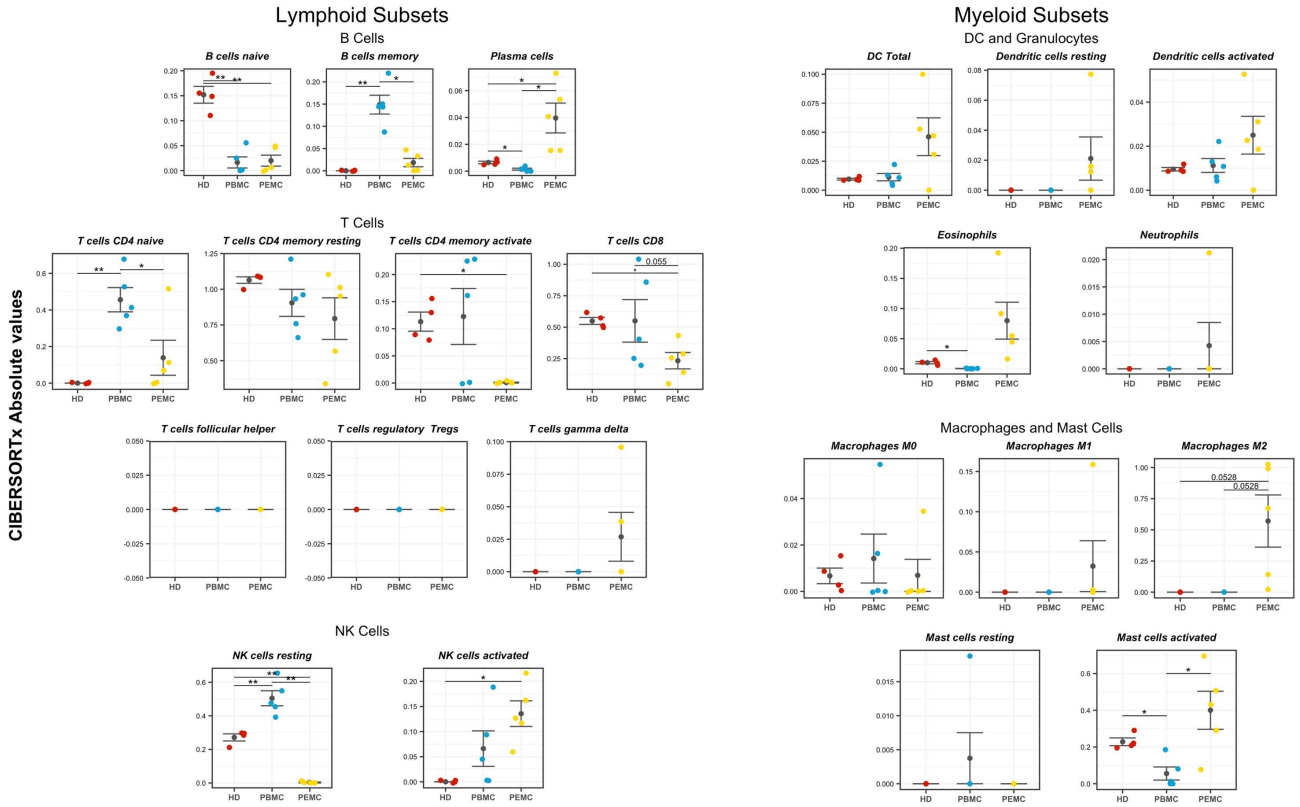
Lymphoid Subsets
B Cells
B cells naive
B cells memory
Plasma cells
T Cells
T cells CD4 naive
T cells CD4 memory resting
T cells CD4 memory activate
T cells CD8
T cells follicular helper
T cells regulatory Tregs
T cells gamma delta
NK Cells
NK cells resting
NK cells activated
CIBERSORTx Absolute values
Myeloid Subsets
DC and Granulocytes
DC Total
Dendritic cells resting
Dendritic cells activated
Eosinophils
Neutrophils
Macrophages and Mast Cells
Macrophages M0
Macrophages M1
Macrophages M2
Mast cells resting
Mast cells activated
HD
PBMC
PEMC

Figure S3

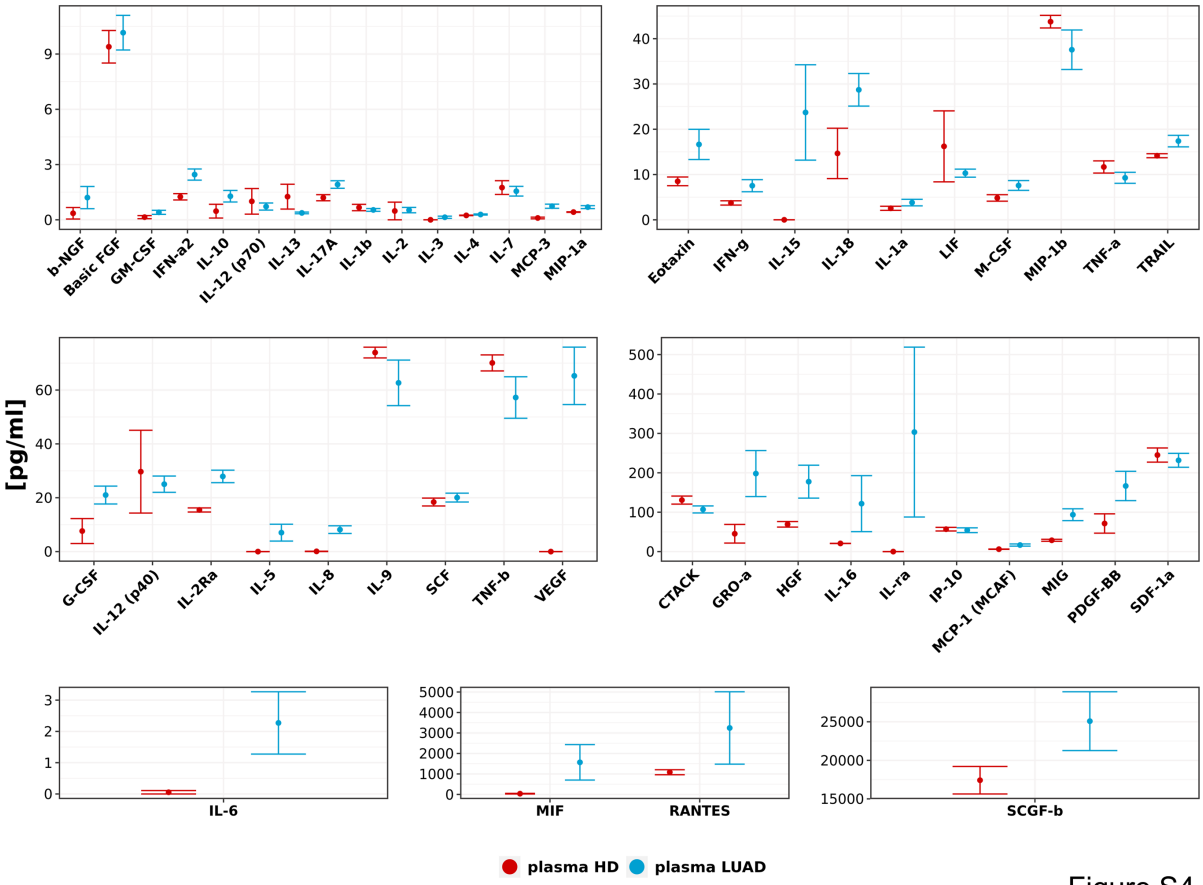
[pg/ml]
b-NGF
Basic FGF
GM-CSF
IFN-a2
IL-10
IL-12 (p70)
IL-13
IL-17A
IL-1b
IL-2
IL-3
IL-4
IL-7
MCP-3
MIP-1a
Eotaxin
IFN-g
IL-15
IL-18
IL-1a
LIF
M-CSF
MIP-1b
TNF-a
TRAIL
G-CSF
IL-12 (p40)
IL-2Ra
IL-5
IL-8
IL-9
SCF
TNF-b
VEGF
CTACK
GRO-a
HGF
IL-16
IL-ra
IP-10
MCP-1 (MCAF)
MIG
PDGF-BB
SDF-1a
IL-6
MIF
RANTES
SCGF-b
plasma HD
plasma LUAD

Figure S4

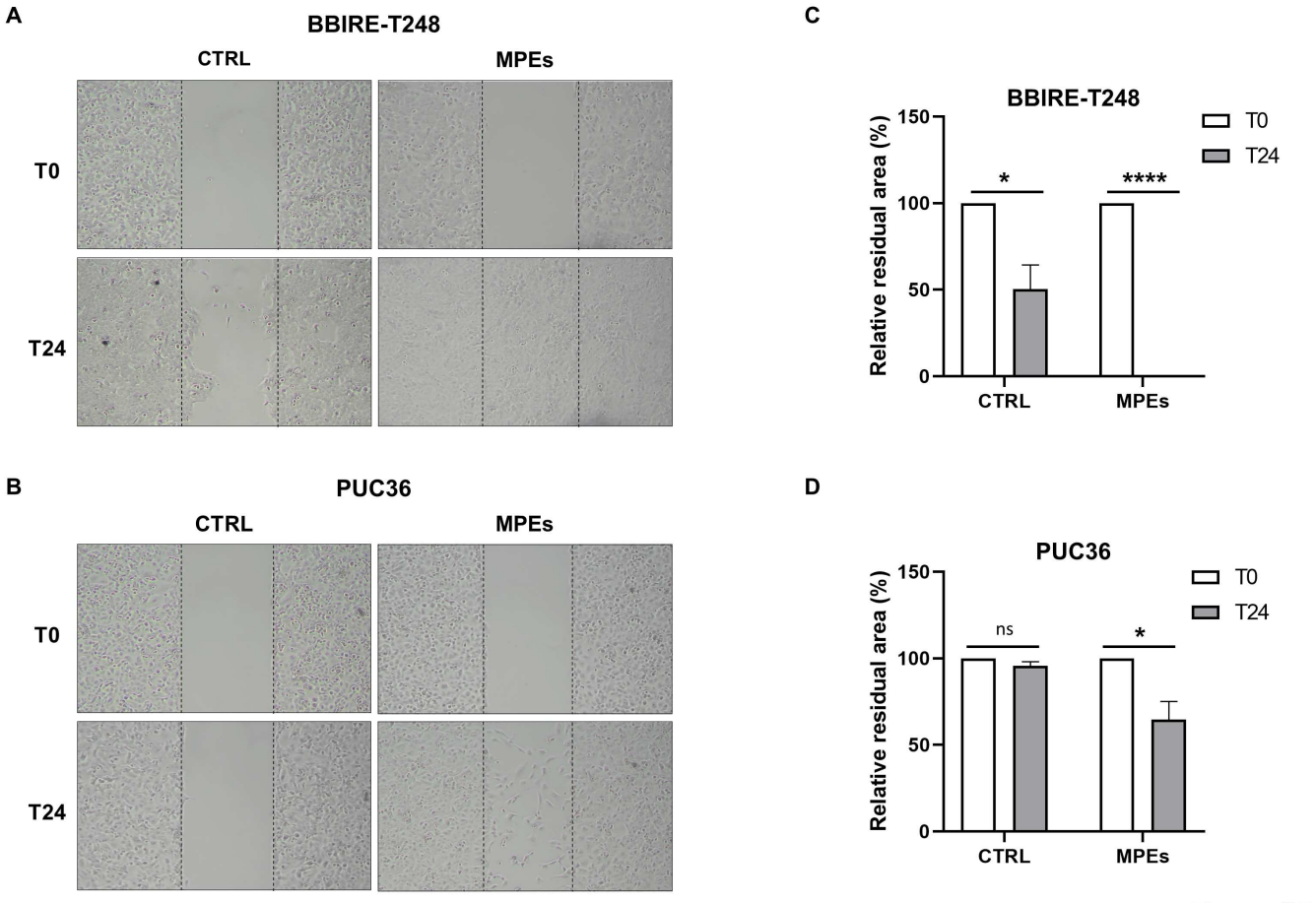
A
BBIRE-T248
CTRL
MPEs
T0
T24
B
PUC36
CTRL
MPEs
T0
T24
C
BBIRE-T248
Relative residual area (%)
150
100
50
0
*
****
T0
T24
CTRL
MPEs
D
PUC36
Relative residual area (%)
150
100
50
0
ns
*
T0
T24
CTRL
MPEs

Figure S5

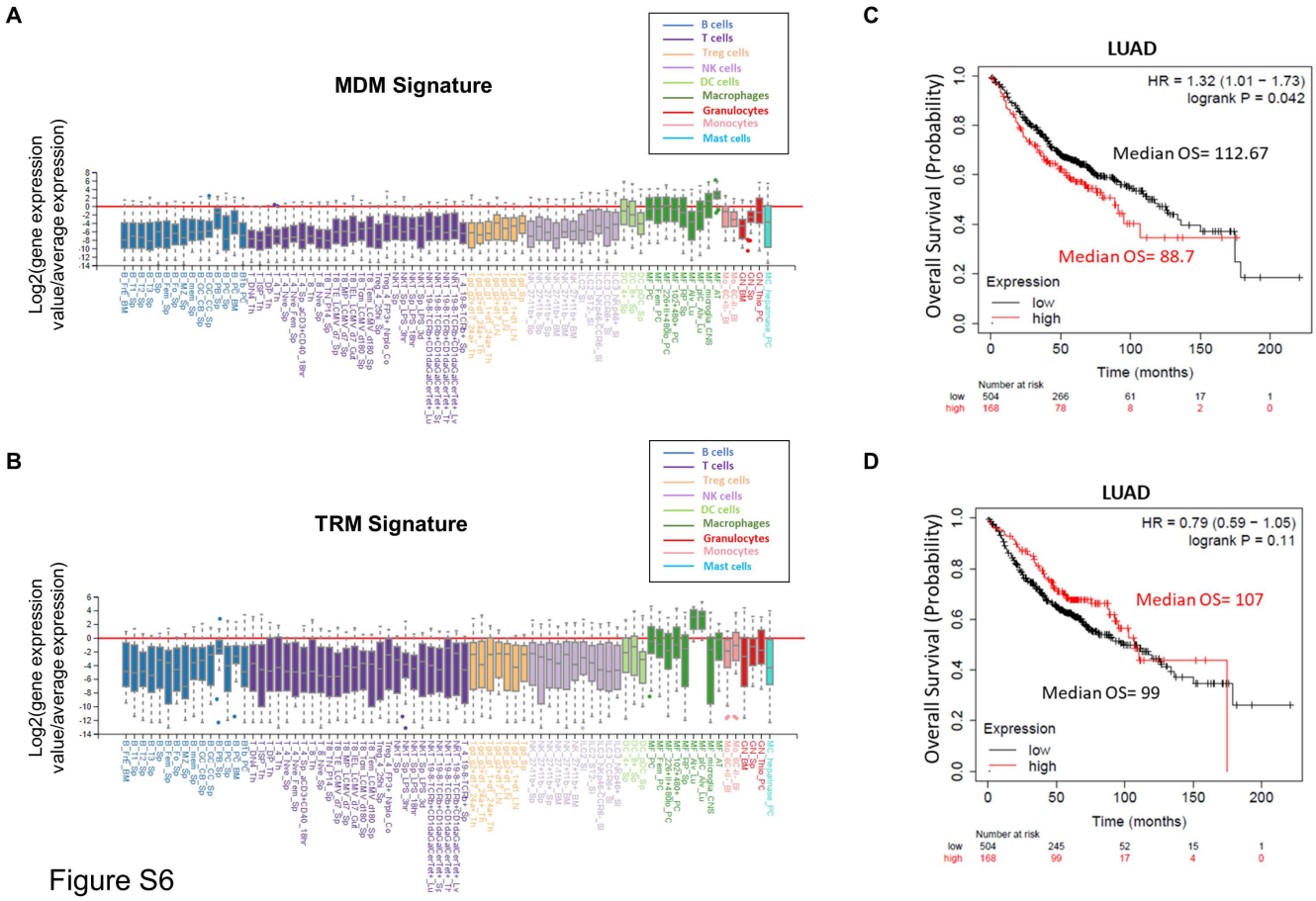
A
MDM Signature
B cells
T cells
Treg cells
NK cells
DC cells
Macrophages
Granulocytes
Monocytes
Mast cells
Log2(gene expression value/average expression)
B
TRM Signature
C
LUAD
HR = 1.32 (1.01 − 1.73)
logrank P = 0.042
Median OS= 112.67
Median OS= 88.7
Expression
low
high
Overall Survival (Probability)
Time (months)
Number at risk
low 504 266 61 17 1
high 168 78 8 2 0
D
LUAD
HR = 0.79 (0.59 − 1.05)
logrank P = 0.11
Median OS= 107
Median OS= 99
Expression
low
high
Overall Survival (Probability)
Time (months)
Number at risk
low 504 245 52 15 1
high 168 99 17 4 0

Figure S6

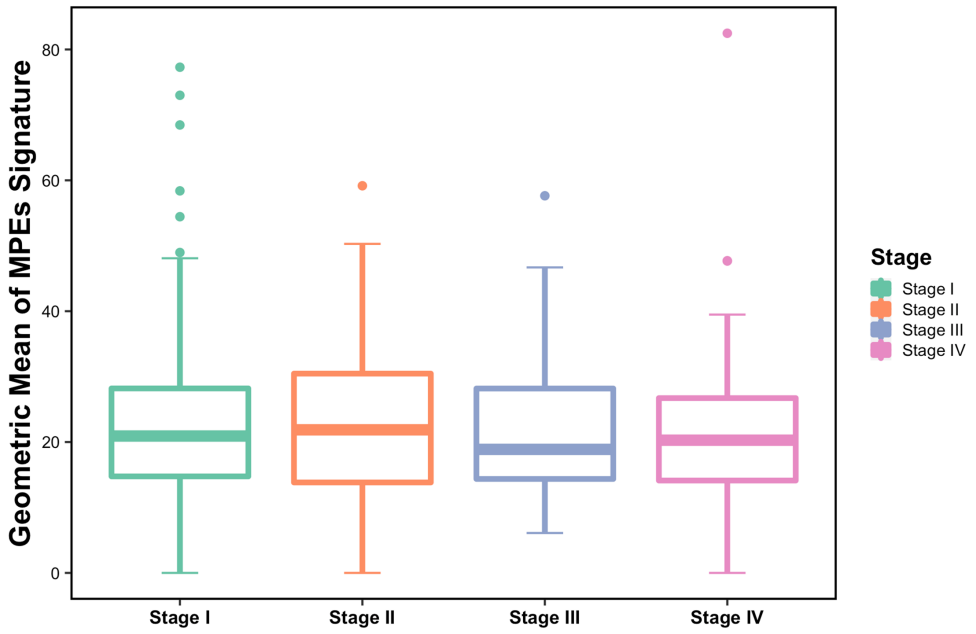
Geometric Mean of MPEs Signature
80
60
40
20
0
Stage I
Stage II
Stage III
Stage IV
Stage
Stage I
Stage II
Stage III
Stage IV

Figure S7